Title

A high-resolution HLA reference panel capturing global population diversity enables multi-ancestry fine-mapping in HIV host response

Journal

Nature Genetics, 53(10)

ISSN

1061-4036

Authors

Luo, Yang

Kanai, Masahiro

Choi, Wanson

et al.

Publication Date

2021-10-01

DOI

10.1038/s41588-021-00935-7

Peer reviewed

HHS Public Access

Author manuscript

Nat Genet. Author manuscript; available in PMC 2022 April 05.

Published in final edited form as:

Nat Genet. 2021 October ; 53(10): 1504–1516. doi:10.1038/s41588-021-00935-7.

* yangluo@broadinstitute.org, soumya@broadinstitute.org.

Author Contributions

Y.L. and S.R. conceived, designed and performed analyses, wrote the manuscript and supervised the research. M.K. implemented the omnibus test for the HIV-1 fine-mapping study. Y.L., W.C., M.K., P.E.S., J.T.E., and B.H. contributed to the development of the HLA-TAPAS pipeline. X.L. performed the selection analysis. S. Sakaue performed imputation comparison between Beagle v.4 and Minimac4. L.F., S. Schoenherr, C.F and A.V.S. hosted the HLA imputation server. J.T.E, M.G.-A. and P.K.G helped with the GaP data acquisition. K.Y., K.O., D.W.H., X.G., N.D.P., Y.-D.I.C., J.I.R., K.D.T., S.S.R., A.C., J.G.W., S.K., M.H.C., A.M., T.E., and Y.O. contributed to the WGS data acquisition. J.F., M.C. and P.J.M contributed to the HIV-1 data acquisition. All authors contributed to the writing of the manuscript.

NHLBI Trans-Omics for Precision Medicine (TOPMed) Consortium

Namiko Abe[40], Gonçalo Abecasis[41], Francois Aguet[42], Christine Albert[43], Laura Almasy[44], Alvaro Alonso[45], Seth Ament[46], Peter Anderson[47], Pramod Anugu[48], Deborah Applebaum-Bowden[49], Kristin Ardlie[42], Dan Arking[50], Donna K. Arnett[51], Allison Ashley-Koch[52], Stella Aslibekyan[53], Tim Assimes[54], Paul Auer[55], Dimitrios Avramopoulos[50], Najib Ayas[56], Adithya Balasubramanian[57], John Barnard[58], Kathleen Barnes[59], R. Graham Barr[60], Emily Barron-Casella[50], Lucas Barwick[61], Terri Beaty[50], Gerald Beck[58], Diane Becker[50], Lewis Becker[50], Rebecca Beer[62], Amber Beitelshees[46], Emelia Benjamin[63], Takis Benos[64], Marcos Bezerra[65], Larry Bielak[41], Joshua Bis[47], Thomas Blackwell[41], John Blangero[66], Eric Boerwinkle[67], Donald W. Bowden[68], Russell Bowler[69], Jennifer Brody[47], Ulrich Broeckel[70], Jai Broome[47], Deborah Brown[67], Karen Bunting[40], Esteban Burchard[71], Carlos Bustamante[54], Erin Buth[47], Brian Cade[72], Jonathan Cardwell[73], Vincent Carey[72], Julie Carrier[74], Cara Carty[75], Richard Casaburi[76], Juan P. Casas Romero[72], James Casella[50], Peter Castaldi[72], Mark Chaffin[42], Christy Chang[46], Yi-Cheng Chang[77], Daniel Chasman[72], Sameer Chavan[73], Bo-Juen Chen[40], Wei-Min Chen[78], Yii-Der Ida Chen[26], Michael H. Cho[33], Seung Hoan Choi[42], Lee-Ming Chuang[77], Mina Chung[58], Ren-Hua Chung[79], Clary Clish[42], Suzy Comhair[58], Matthew Conomos[47], Elaine Cornell[80], Adolfo Correa[29], Carolyn Crandall[76], James Crapo[69], L. Adrienne Cupples[81], Joanne Curran[66], Jeffrey Curtis[41], Brian Custer[82], Coleen Damcott[46], Dawood Darbar[83], Sean David[84], Colleen Davis[47], Michelle Daya[73], Mariza de Andrade[85], Lisa de las Fuentes[86], Paul de Vries[67], Michael DeBaun[87], Ranjan Deka[88], Dawn DeMeo[72], Scott Devine[46], Huyen Dinh[57], Harsha Doddapaneni[57], Qing Duan[89], Shannon Dugan-Perez[57], Ravi Duggirala[66], Jon Peter Durda[80], Susan K. Dutcher[86], Charles Eaton[90], Lynette Ekunwe[48], Adel El Boueiz[91], Patrick Ellinor[92], Leslie Emery[47], Serpil Erzurum[58], Charles Farber[78], Jesse Farek[57], Tasha Fingerlin[69], Matthew Flickinger[41], Myriam Fornage[67], Nora Franceschini[89], Chris Frazar[47], Mao Fu[46], Stephanie M. Fullerton[47], Lucinda Fulton[86], Stacey Gabriel[42], Weiniu Gan[62], Shanshan Gao[73], Yan Gao[48], Margery Gass[93], Heather Geiger[40], Bruce Gelb[94], Mark Geraci[64], Soren Germer[40], Robert Gerszten[95], Auyon Ghosh[72], Richard Gibbs[57], Chris Gignoux[54], Mark Gladwin[64], David Glahn[96], Stephanie Gogarten[47], Da-Wei Gong[46], Harald Goring[66], Sharon Graw[59], Kathryn J. Gray[97], Daniel Grine[73], Colin Gross[41], C. Charles Gu[86], Yue Guan[46], Xiuqing Guo[26], Namrata Gupta[42], David M. Haas[98], Jeff Haessler[93], Michael Hall[48], Yi Han[57], Patrick Hanly[99], Daniel Harris[46], Nicola L. Hawley[100], Jiang He[101], Ben Heavner[47], Susan Heckbert[47], Ryan Hernandez[71], David Herrington[68], Craig Hersh[72], Bertha Hidalgo[53], James Hixson[67], Brian Hobbs[72], John Hokanson[73], Elliott Hong[46], Karin Hoth[102], Chao (Agnes) Hsiung[79], Jianhong Hu[57], Yi-Jen Hung[103], Haley Huston[104], Chii Min Hwu[105], Marguerite Ryan Irvin[53], Rebecca Jackson[106], Deepti Jain[47], Cashell Jaquish[62], Jill Johnsen[104], Andrew Johnson[62], Craig Johnson[47], Rich Johnston[45], Kimberly Jones[50], Hyun Min Kang[41], Robert Kaplan[107], Sharon Kardia[41], Shannon Kelly[71], Eimear Kenny[94], Michael Kessler[46], Alyna Khan[47], Ziad Khan[57], Wonji Kim[108], John Kimoff[109], Greg Kinney[73], Barbara Konkle[104], Charles Kooperberg[93], Holly Kramer[110], Christoph Lange[111], Ethan Lange[73], Leslie Lange[73], Cathy Laurie[47], Cecelia Laurie[47], Meryl LeBoff[72], Jiwon Lee[72], Sandra Lee[57], Wen-Jane Lee[105], Jonathon LeFaive[41], David Levine[47], Dan Levy[62], Joshua Lewis[46], Xiaohui Li[112], Yun Li[89], Henry Lin[112], Honghuang Lin[81], Xihong Lin[111], Simin Liu[90], Yongmei Liu[52], Yu Liu[54], Ruth J. F. Loos[94], Steven Lubitz[92], Kathryn Lunetta[81], James Luo[62], Ulysses Magalang[113], Michael Mahaney[66], Barry Make[50], Ani Manichaikul[78], Alisa Manning[114], JoAnn Manson[72], Lisa Martin[115], Melissa Marton[40], Susan Mathai[73], Rasika Mathias[50], Susanne May[47], Patrick McArdle[46], Merry-Lynn McDonald[53], Sean McFarland[108], Stephen McGarvey[90], Daniel McGoldrick[47], Caitlin McHugh[47], Becky McNeil[116], Hao Mei[48], James Meigs[92], Vipin Menon[57], Luisa Mestroni[59], Ginger Metcalf[57], Deborah A. Meyers[117], Emmanuel Mignot[54], Julie Mikulla[62], Nancy Min[48], Mollie Minear[118], Ryan L. Minster[64], Braxton D. Mitchell[46], Matt Moll[72], Zeineen Momin[57], May E. Montasser[46], Courtney Montgomery[119], Donna Muzny[57], Josyf C. Mychaleckyj[78], Girish Nadkarni[94], Rakhi Naik[50], Take Naseri[120], Pradeep Natarajan[42], Sergei Nekhai[121], Sarah C. Nelson[47], Bonnie Neltner[73], Caitlin Nessner[57], Deborah Nickerson[47], Osuji Nkechinyere[57], Kari North[89], Jeff O'Connell[46], Tim O'Connor[46], Heather Ochs-Balcom[122], Geoffrey Okwuonu[57], Allan Pack[123], David T. Paik[54], Nicholette D. Palmer[27], James Pankow[124], George Papanicolaou[62], Cora Parker[116], Gina Peloso[81], Juan Manuel Peralta[66], Marco Perez[54], James Perry[46], Ulrike Peters[93], Patricia Peyser[41], Lawrence S. Phillips[45], Jacob Pleiness[41], Toni Pollin[46], Wendy Post[50], Julia Powers Becker[73], Meher Preethi Boorgula[73], Michael Preuss[94], Bruce Psaty[47], Pankaj Qasba[62], Dandi Qiao[72], Zhaohui Qin[45], Nicholas Rafaels[73], Laura Raffield[89], Mahitha Rajendran[57], Vasan S. Ramachandran[81], D. C. Rao[86], Laura Rasmussen-Torvik[125], Aakrosh Ratan[78], Susan Redline[72], Robert Reed[46], Catherine Reeves[40], Elizabeth Regan[69], Alex Reiner[126], Muagututi'a Sefuiva Reupena[127], Ken Rice[47], Stephen S. Rich[28], Rebecca Robillard[128], Nicolas Robine[40], Dan Roden[87], Carolina Roselli[42], Jerome I. Rotter[26], Ingo Ruczinski[50], Alexi Runnels[40], Pamela Russell[73], Sarah Ruuska[104], Kathleen Ryan[46], Ester Cerdeira Sabino[129], Danish Saleheen[60], Shabnam Salimi[46], Sejal Salvi[57], Steven Salzberg[50], Kevin Sandow[112], Vijay G. Sankaran[130], Jireh Santibanez[57], Karen Schwander[86], David Schwartz[73], Frank Sciurba[64], Christine Seidman[131], Jonathan Seidman[131], Frédéric Sériès[132], Vivien Sheehan[45], Stephanie L. Sherman[45], Amol Shetty[46], Aniket Shetty[73], Wayne Hui-Heng Sheu[105], M. Benjamin Shoemaker[87], Brian Silver[133], Edwin Silverman[72], Robert Skomro[134], Albert V. Smith[17,18], Jennifer Smith[41], Josh Smith[47], Nicholas Smith[47],

A high-resolution HLA reference panel capturing global population diversity enables multi-ancestry fine-mapping in HIV host response

Tanja Smith[40], Sylvia Smoller[107], Beverly Snively[68], Michael Snyder[54], Tamar Sofer[72], Nona Sotoodehnia[47], Adrienne M. Stilp[47], Garrett Storm[73], Elizabeth Streeten[46], Jessica Lasky Su[72], Yun Ju Sung[86], Jody Sylvia[72], Adam Szpiro[47], Daniel Taliun[41], Hua Tang[54], Margaret Taub[50], Kent D. Taylor[26], Matthew Taylor[59], Simeon Taylor[46], Marilyn Telen[52], Timothy A. Thornton[47], Machiko Threlkeld[47], Lesley Tinker[93], David Tirschwell[47], Sarah Tishkoff[123], Hemant Tiwari[53], Catherine Tong[47], Russell Tracy[80], Michael Tsai[124], Dhananjay Vaidya[50], David Van Den Berg[135], Peter VandeHaar[41], Scott Vrieze[124], Tarik Walker[73], Robert Wallace[102], Avram Walts[73], Fei Fei Wang[47], Heming Wang[136], Jiongming Wang[41], Karol Watson[76], Jennifer Watt[57], Daniel E. Weeks[64], Joshua Weinstock[41], Bruce Weir[47], Scott T. Weiss[72], Lu-Chen Weng[92], Jennifer Wessel[98], Cristen Willer[41], Kayleen Williams[47], L. Keoki Williams[137], Carla Wilson[72], James Wilson[95], Lara Winterkorn[40], Quenna Wong[47], Joseph Wu[54], Huichun Xu[46], Lisa Yanek[50], Ivana Yang[73], Ketian Yu[41], Seyedeh Maryam Zekavat[42], Yingze Zhang[64], Snow Xueyan Zhao[69], Wei Zhao[41], Xiaofeng Zhu[138], Michael Zody[40], and Sebastian Zoellner[41] [40]New York Genome Center, New York, NY, USA. [41]University of Michigan, Ann Arbor, MI, USA. [42]Broad Institute, Cambridge, MA, USA. [43]Brigham and Women's Hospital, Cedars Sinai Boston, MA, USA. [44]Children's Hospital of Philadelphia, University of Pennsylvania, Philadelphia, PA, USA. [45]Emory University, Atlanta, GA, USA. [46]University of Maryland, Baltimore, MD, USA. [47]University of Washington, Seattle, WA, USA. [48]University of Mississippi, Jackson, MS, USA. [49]National Institutes of Health, Bethesda, MD, USA. [50]Johns Hopkins University, Baltimore, MD, USA. [51]University of Kentucky, Lexington, KY, USA. [52]Duke University, Durham, NC, USA. [53]University of Alabama, Birmingham, AL, USA. [54]Stanford University, Stanford, CA, USA. [55]University of Wisconsin Milwaukee, Milwaukee, WI, USA. [56]Providence Health Care Research Institute, Vancouver, BC, Canada. [57]Baylor College of Medicine Human Genome Sequencing Center, Houston, TX, USA. [58]Cleveland Clinic, Cleveland, OH, USA. [59]University of Colorado Anschutz Medical Campus, Aurora, CO, USA. [60]Columbia University, New York, NY, USA. [61]The Emmes Corporation, Rockville, MD, USA. [62]National Heart, Lung, and Blood Institute, National Institutes of Health, Bethesda, MD, USA. [63]Boston University, Massachusetts General Hospital, Boston, MA, USA. [64]University of Pittsburgh, Pittsburgh, PA, USA. [65]Fundação de Hematologia e Hemoterapia de Pernambuco – Hemope, Recife, Brazil. [66]University of Texas Rio Grande Valley School of Medicine, Brownsville, TX, USA. [67]University of Texas Health at Houston, Houston, TX, USA. [68]Wake Forest Baptist Health, Winston-Salem, NC, USA. [69]National Jewish Health, Denver, CO, USA. [70]Medical College of Wisconsin, Milwaukee, WI, USA. [71]University of California, San Francisco, San Francisco, CA, USA. [72]Brigham & Women's Hospital, Boston, MA, USA. [73]University of Colorado at Denver, Denver, CO, USA. [74]University of Montreal, Montreal, QC, Canada. [75]Washington State University, Seattle, WA, USA. [76]University of California, Los Angeles, Los Angeles, CA, USA. [77]National Taiwan University, Taipei, Taiwan. [78]University of Virginia, Charlottesville, VA, USA. [79]National Health Research Institutes, Zhunan, Taiwan. [80]University of Vermont, Burlington, VT, USA. [81]Boston University, Boston, MA, USA. [82]Vitalant Research Institute, San Francisco, CA, USA. [83]University of Illinois at Chicago, Chicago, IL, USA. [84]University of Chicago, Chicago, IL, USA. [85]Mayo Clinic, Rochester, MN, USA. [86]Washington University in St Louis, St Louis, MO, USA. [87]Vanderbilt University, Nashville, TN, USA. [88]University of Cincinnati, Cincinnati, OH, USA. [89]University of North Carolina, Chapel Hill, NC, USA. [90]Brown University, Providence, RI, USA. [91]Channing Division of Network Medicine, Harvard University, Boston, MA, USA. [92]Massachusetts General Hospital, Boston, MA. [93]Fred Hutchinson Cancer Research Center, Seattle, WA, USA. [94]Icahn School of Medicine at Mount Sinai, New York, NY, USA. [95]Beth Israel Deaconess Medical Center, Boston, MA, USA. [96]Boston Children's Hospital, Harvard Medical School, Boston, MA, USA. [97]Mass General Brigham, Boston, MA, USA. [98]Indiana University, Indianapolis, IN, USA. [99]University of Calgary, Calgary, AB, Canada. [100]Yale University, New Haven, CT, USA. [101]Tulane University, New Orleans, LA, USA. [102]University of Iowa, Iowa City, IA, USA. [103]Tri-Service General Hospital National Defense Medical Center, Taipei, Taiwan. [104]Bloodworks Northwest, Seattle, WA, USA. [105]Taichung Veterans General Hospital Taiwan, Taichung, Taiwan. [106]Oklahoma State University Medical Center, Tulsa, OK, USA. [107]Albert Einstein College of Medicine, Bronx, NY, USA. [108]Harvard University, Cambridge, MA, USA. [109]McGill University, Montreal, QC, Canada. [110]Loyola University, Chicago, IL, USA. [111]Harvard School of Public Health, Boston, MA, USA. [112]Lundquist Institute, Torrence, CA, USA. [113]Ohio State University, Columbus, OH, USA. [114]Broad Institute, Harvard University, Massachusetts General Hospital, Cambridge, MA, USA. [115]George Washington University, Washington, D.C., USA. [116]RTI International, Durham, NC, USA. [117]University of Arizona, Tucson, AZ, USA. [118]National Institute of Child Health and Human Development, National Institutes of Health, Bethesda, MD, USA. [119]Oklahoma Medical Research Foundation, Oklahoma City, OK, USA. [120]Ministry of Health, Government of Samoa, Apia, Samoa. [121]Howard University, Washington, D.C., USA. [122]University at Buffalo, Buffalo, NY, USA. [123]University of Pennsylvania, Philadelphia, PA, USA. [124]University of Minnesota, Minneapolis, MN, USA. [125]Northwestern University, Chicago, IL, USA. [126]Fred Hutchinson Cancer Research Center, University of Washington, Seattle, WA, USA. [127]Lutia I Puava Ae Mapu I Fagalele, Apia, Samoa. [128]University of Ottawa, Ottawa, ON, Canada. [129]Universidade de Sao Paulo, Sao Paulo, Brazil. [130]Division of Hematology/Oncology, Broad Institute, Harvard University, Boston, MA, USA. [131]Harvard Medical School, Boston, MA, USA. [132]Université Laval, Quebec City, QC, Canada. [133]University of Massachusetts Memorial Medical Center, Worcester, MA, USA. [134]University of Saskatchewan, Saskatoon, SK, Canada. [135]University of Southern California, Los Angeles, CA, USA. [136]Brigham and Women's Hospital, Partners, Boston, MA, USA. [137]Henry Ford Health System, Detroit, MI, USA. [138]Case Western Reserve University, Cleveland, OH, USA.

Yang Luo[1,2,3,4,5,*], **Masahiro Kanai**[4,5,6,7,8], **Wanson Choi**[9], **Xinyi Li**[10], **Saori Sakaue**[1,2,3,4,5], **Kenichi Yamamoto**[8,11], **Kotaro Ogawa**[8,12], **Maria Gutierrez-Arcelus**[1,2,3,4,5], **Peter K. Gregersen**[13], **Philip E. Stuart**[14], **James T. Elder**[14,15], **Lukas Forer**[16], **Sebastian Schoenherr**[16], **Christian Fuchsberger**[16,17,18,19], **Albert V. Smith**[17,18], **Jacques Fellay**[20,21], **Mary Carrington**[22,23], **David W. Haas**[24,25], **Xiuqing Guo**[26], **Nicholette D. Palmer**[27], **Yii-Der Ida Chen**[26], **Jerome I. Rotter**[26], **Kent D. Taylor**[26], **Stephen S. Rich**[28], **Adolfo Correa**[29], **James G. Wilson**[30], **Sekar Kathiresan**[5,31,32], **Michael H. Cho**[33], **Andres Metspalu**[34], **Tonu Esko**[5,34], **Yukinori Okada**[8,35], **Buhm Han**[36], **NHLBI Trans-Omics for Precision Medicine (TOPMed) Consortium**, **Paul J. McLaren**[37,38], **Soumya Raychaudhuri**[1,2,3,4,5,39,*]

[1]Center for Data Sciences, Brigham and Women's Hospital, Harvard Medical School, Boston, MA, USA.

[2]Division of Rheumatology, Immunology, and Immunity, Brigham and Women's Hospital, Harvard Medical School, Boston, MA, USA.

[3]Division of Genetics, Brigham and Women's Hospital, Harvard Medical School, Boston, MA, USA.

[4]Department of Biomedical Informatics, Harvard Medical School, Boston, MA, USA.

[5]Broad Institute of MIT and Harvard, Cambridge, MA, USA.

[6]Analytic and Translational Genetics Unit, Massachusetts General Hospital, Boston, MA, USA.

[7]Stanley Center for Psychiatric Research, Broad Institute of Harvard and MIT, Cambridge, MA, USA.

[8]Department of Statistical Genetics, Osaka University Graduate School of Medicine, Suita, Japan.

[9]Department of Biomedical Sciences, Seoul National University College of Medicine, Seoul, South Korea.

[10]Committee on Genetics, Genomics, and Systems Biology, University of Chicago, Chicago, IL, USA.

[11]Department of Pediatrics, Osaka University Graduate School of Medicine, Osaka, Japan.

[12]Department of Neurology, Osaka University Graduate School of Medicine, Osaka, Japan.

[13]The Robert S. Boas Center for Genomics and Human Genetics, Feinstein Institute for Medical Research, North Short LIJ Health System, Manhasset, NY, USA.

[14]Department of Dermatology, University of Michigan, Ann Arbor, MI, USA.

[15]Ann Arbor Veterans Affairs Hospital, Ann Arbor, MI, USA.

[16]Institute of Genetic Epidemiology, Department of Genetics and Pharmacology, Medical University of Innsbruck, Innsbruck, Austria.

[17]Department of Biostatistics, University of Michigan School of Public Health, Ann Arbor, MI, USA.

[18]Center for Statistical Genetics, University of Michigan School of Public Health, Ann Arbor, MI, USA.

[19]Institute for Biomedicine, Eurac Research, Bolzano, Italy.

[20]Precision Medicine Unit, Lausanne University Hospital and University of Lausanne, Lausanne, Switzerland.

[21]School of Life Sciences, EPFL, Lausanne, Switzerland.

[22]Basic Science Program, Frederick National Laboratory for Cancer Research, Frederick, MD, USA.

[23]Ragon Institute of MGH, MIT and Harvard, Boston, MA, USA.

[24]Vanderbilt University Medical Center, Nashville, TN, USA.

[25]Meharry Medical College, Nashville, TN, USA.

[26]The Institute for Translational Genomics and Population Sciences, Department of Pediatrics, The Lundquist Institute for Biomedical Innovation at Harbor-UCLA Medical Center, Torrance, CA, USA.

[27]Department of Biochemistry, Wake Forest School of Medicine, Winston-Salem, NC, USA.

[28]Center for Public Health Genomics, University of Virginia School of Medicine, Charlottesville, VA, USA.

[29]Medicine, University of Mississippi Medical Center, Jackson, MS, USA.

[30]Physiology and Biophysics, University of Mississippi Medical Center, Jackson, MS, USA.

[31]Center for Genomic Medicine, Massachusetts General Hospital, Boston, MA, USA.

[32]Cardiology Division of the Department of Medicine, Massachusetts General Hospital, Boston, MA, USA

[33]Channing Division of Network Medicine, Department of Medicine, Brigham and Women's Hospital, Harvard Medical School, Boston, MA, USA.

[34]Estonian Genome Center, Institute of Genomics, University of Tartu, Tartu, Estonia.

[35]Laboratory of Statistical Immunology, Immunology Frontier Research Center (WPI-IFReC), Osaka University, Suita, Japan.

[36]Department of Medical Sciences, Seoul National University College of Medicine, Seoul, South Korea.

[37]J.C. Wilt Infectious Diseases Research Centre, National Microbiology Laboratories, Public Health Agency of Canada, Winnipeg, MB, Canada.

[38]Department of Medical Microbiology and Infectious Diseases, University of Manitoba, Winnipeg, MB, Canada.

[39]Centre for Genetics and Genomics Versus Arthritis, University of Manchester, Manchester, UK.

Abstract

Fine-mapping to plausible causal variation may be more effective in multi-ancestry cohorts, particularly in the MHC, which has population-specific structure. To enable such studies, we constructed a large (n = 21,546) HLA reference panel spanning five global populations based on

whole-genome sequences. Despite population specific long-range haplotypes, we demonstrated accurate imputation at G-group resolution (94.2%, 93.7%, 97.8% and 93.7% in Admixed African (AA), East Asian (EAS), European (EUR) and Latino (LAT) populations). Applying HLA imputation to genome-wide association study (GWAS) data for HIV-1 viral load in three populations (EUR, AA and LAT), we obviated effects of previously reported associations from population-specific HIV studies and discovered a novel association at position 156 in HLA-B. We pinpointed the MHC association to three amino acid positions (97, 67 and 156) marking three consecutive pockets (C, B and D) within the HLA-B peptide binding groove, explaining 12.9% of trait variance.

The human leukocyte antigen (HLA) genes located within the major histocompatibility complex (MHC) region encode proteins that play essential roles in immune responses, including antigen presentation. They account for more heritability than all other variants together for many diseases[1–4]. It also has more reported GWAS trait associations than any other locus[5]. The extended MHC region spans 6 Mb on chromosome 6p21.3 and contains more than 260 genes[6]. It is striking for its structural diversity and long-range linkage equilibrium (LD). Due to population-specific positive selection, it harbors unusually high sequence variation, longer haplotypes than most of the genome, and haplotypes that are specific to individual ancestral populations[7–9]. Consequently, the MHC is among the most challenging regions in the genome to analyze. Advances in HLA imputation[10–12] have enabled MHC association and fine-mapping studies at single gene and long-range haplotype level[2,13–16]. But despite large effect sizes, fine-mapping in multiple populations simultaneously is challenging without a single large and high-resolution multi-ancestry reference panel. This has caused confusion in some instances. For example, the Human Immunodeficiency Virus (HIV) resulted in 38.0 million people living with HIV infection in 2019, and led to 770,000 deaths in 2018 alone[17]. Multiple risk HLA risk alleles have been independently reported in different populations[1,14,18], and it remains unclear if they represent truly population-specific signals or are confounded by high LD in the region.

Results

Performance evaluation of inferred classical *HLA* alleles.

To build a large-scale multi-ancestry HLA imputation reference panel, we used high-coverage whole genome sequencing (WGS) datasets[19–23] from the Japan Biological Informatics Consortium[22], the BioBank Japan Project[20], the Estonian Biobank[24], the 1000 Genomes Project (1KG)[23] and a subset of studies in the TOPMed program (Supplementary Note and Supplementary Tables 1 and 2). To perform HLA typing using WGS data, we extracted reads mapped to the extended MHC region (chr6:25Mb-35Mb) and unmapped reads from 21,546 individuals. We applied a population reference graph[25–27] for the MHC region to infer classical alleles for three HLA class I genes (*HLA-A, -B* and *-C*) and five class II genes (*HLA-DQA1*, *-DQB1*, *-DRB1*, *-DPA1* and *-DPB1*) at G-group resolution, which determines the sequences of the exons encoding the peptide binding groove (Extended Data Fig. 1). We required samples to have >20x coverage across all HLA genes (Supplementary Tables 1 and 3). After quality control, our panel included 10,187 EUR, 7,849 AA, 2,069 EAS, 952 LAT and 489 South Asian (SAS) individuals.

To assess the accuracy of the WGS *HLA* allele calls, we compared the inferred *HLA* classical alleles to gold standard sequence-based typing (SBT) in 955 1KG individuals and 288 Japanese individuals and quantified concordance. In both cohorts, we observed slightly higher average accuracy for class I genes, obtaining 99.0% (one-field, formally known as two-digit), 99.2% (amino acid) and 96.5% (G-group resolution), than class II genes, obtaining 98.7% (one-field), 99.7% (amino acid) and 96.7% (G-group resolution) (Methods, Supplementary Fig. 1, Supplementary Tables 4 and 5, and Supplementary Data 1).

HLA reference panel construction and evaluation.

Next, we constructed a multi-ancestry HLA imputation reference panel based on classical *HLA* alleles and 38,398 genomic markers in the extended MHC region using a novel HLA-focused pipeline HLA-TAPAS (HLA-Typing At Protein for Association Studies; see Code availability). Briefly, HLA-TAPAS can handle HLA reference panel construction (*MakeReference*), HLA imputation (*SNP2HLA*) and HLA association (*HLAassoc*) (Fig. 1 and Methods). Compared to a widely used HLA reference panel with European-only individuals (The Type 1 Diabetes Genetics Consortium[11], T1DGC), this new reference panel has a six-fold increase in the number of observed *HLA* alleles and non-HLA genomic markers (Supplementary Table 6). We noted the difference in observed classical *HLA* alleles is mainly due to the inclusion of diverse populations rather than its size; after downsampling the reference panel to be the same size as T1DGC (n = 5,225), there was still a three-fold increase in observed alleles (Fig. 2a).

To empirically assess imputation accuracy of our reference panel, we first used the publicly available gold-standard *HLA* types (*HLA-A*, *-B*, *-C*, *-DRB1* and *-DQB1*) of 1,267 diverse samples from AA, EAS, EUR and LAT included in 1KG. We removed 955 overlapping samples within the reference panel, and to ensure a representative analysis we kept 6,007 markers overlapping with the *Global Genotyping Array*. Across the five genes, the average G-group resolution accuracies were 94.2%, 93.7%, 97.8% and 93.7% in AA, EAS, EUR and LAT (Figure 2b,c, Supplementary Table 7, Supplementary Data 2, and Methods). Compared to the T1DGC panel, our multi-ancestry reference panel showed the most improvement for individuals of non-European descent; we obtained 4.27%, 2.96%, 2.90% and 1.05% improvement at G-group resolution for AA, EAS, LAT, and EUR individuals, respectively. Increased diversity was responsible for the improvement; downsampling the reference panel be the same size as the T1DGC panel still yielded superior performance (Fig. 2d). To validate our panel further, we imputed *HLA* alleles into a multi-ancestry cohort of 2,291 individuals from the Genotype and Phenotype (GaP) registry genotyped on the ImmunoChip array. We obtained *HLA* type information for seven classical class I and class II loci (*HLA-A*, *-B*, *-C*, *-DQA1*, *-DQB1*, *-DRB1* and *-DPB1*) in 75 samples with diverse ancestral background (25 EUR, 25 EAS and 25 AA; Supplementary Fig. 2 and Methods). Average accuracies were 99.0%, 95.7% and 97.0% for EUR, EAS and AA, respectively, when comparing SBT *HLA* alleles at G-group resolution (Methods and Supplementary Data 2). Similar to the 1KG analysis, the multi-ancestry reference panel showed significant improvement for individuals with non-European descent (6.3% and 11.1% improvement for EAS and AA individuals, respectively, at G-group resolution), and a more modest 2% improvement in EUR (Supplementary Fig. 3 and Supplementary Table 8). At the amino

acid level, the average accuracies were greater than 99% for all populations, and this accuracy is similar inside and outside the peptide binding groove at six classical HLA genes (Supplementary Table 9).

Fine-mapping causal variants of HIV-1 set point viral load.

Next, we investigated MHC effects within human immunodeficiency virus type 1 (HIV-1) set point viral load. Upon primary infection with HIV-1, the set point viral load is reached after the immune system has developed specific cytotoxic T lymphocytes (CTL) that are able to partially control the virus. It has been well-established that the set point viral load (spVL) varies in the infected population and positively correlates with rate of disease progression[28]. Previous studies suggested that HIV-1 infection has a strong genetic component, and specific HLA class I alleles explain the majority of genetic risk[14,29]. The existence of multiple independent, population-specific, risk-associated alleles has been reported in both European[1,14] and African American[18] populations. However, without a multi-ancestry reference panel, it has not been possible to determine if these signals are consistent across different ancestral groups.

To define the MHC allelic effects shared across multiple populations, we applied our multi-ancestry MHC reference panel to 7,445 EUR, 3,901 AA and 677 LAT HIV-1 infected individuals (Methods and Supplementary Table 10). Imputation resulted in 640 classical *HLA* alleles, 4,513 amino acids in HLA proteins and 49,321 SNPs in the extended MHC region for association and fine-mapping analysis. We confirmed 94.3% and 99.1% imputation accuracy at G-group and amino acid resolution, respectively, for *HLA* alleles with a minor allele frequency > 0.5% in this cohort by comparing imputed classical alleles to the SBT alleles in a subset of 1,067 AA individuals[18] (Extended Data Fig. 2, Supplementary Table 11, and Supplementary Data 2).

We next tested SNPs, amino acid positions and classical *HLA* alleles across the MHC for association to spVL. We performed this jointly in EUR, AA and LAT population using a linear regression model with sex, principal components and ancestry as covariates (Methods). In agreement with previous studies, we found the strongest spVL-associated classical *HLA* allele is *B*57* (effect size = −0.84, $P_{\text{binary}} = 8.68 \times 10^{-144}$). This corresponded to a single residue Val97 in HLA-B that tracks almost perfectly with *B*57* ($r^2 = 0.995$) and showed the strongest association of any single residue (effect size = −0.84, $P_{\text{binary}} = 5.99 \times 10^{-145}$, Extended Data Fig. 3).

To determine which amino acid positions have independent association with spVL, we tested each of the amino acid positions by grouping haplotypes carrying a specific residue at each position in an additive model[2,13] (Methods). We found the strongest spVL-associated amino acid variant in HLA-B is as previously reported[1,14,18] at position 97 (Fig. 3a,b and Supplementary Table 12), which strikingly explains 9.06% of the phenotypic variance. Position 97 in HLA-B was more significant ($P_{\text{omnibus}} = 2.86 \times 10^{-184}$) than any single SNP or classical *HLA* allele, including *B*57* (Extended Data Fig. 3 and Supplementary Data 3). Of the six allelic variants (Val/Asn/Trp/Thr/Arg/Ser) at this position, the Val residue conferred the strongest protective effect (effect size = −0.88, $P = 9.32 \times 10^{-152}$, Supplementary Fig. 4) relative to the most common residue Arg (frequency = 47.8%).

All six amino acid alleles have consistent frequencies and effect sizes across the three population groups (Fig. 4a,b and Extended Data Fig. 4).

We next wanted to test whether there were other independent effects outside of position 97 in HLA-B. After accounting for the effects of amino acid 97 in HLA-B using a conditional haplotype analysis (Methods), we observed a significant independent association at position 67 in HLA-B ($P_{omnibus} = 2.82 \times 10^{-39}$, Fig. 3c,d and Supplementary Table 12). Considering this might be an artifact of forward search, we exhaustively tested all possible pairs of polymorphic amino acid positions in HLA-B. Of 7,260 pairs of amino acid positions, none obtained a better goodness-of-fit than the pair of positions 97 and 67, which collectively explained 11.2% variance in spVL (Fig. 4e and Supplementary Table 13). At position 67, Met67 shows the most protective effect (effect size = −0.44, $P = 1.19 \times 10^{-59}$) among the five possible amino acids (Cys/Phe/Met/Ser/Tyr) relative to the most common residue Ser (frequency = 10.0%).

Conditioning on positions 97 and 67 revealed an additional association at position 156 in HLA-B ($P_{omnibus} = 1.92 \times 10^{-30}$, Fig. 4e,f and Supplementary Table 12). In agreement with the stepwise conditional analysis, when we tested all 287,980 possible combinations of three amino acid positions in HLA-B, the most statistically significant combination of amino acids sites is 67, 97 and 156 ($P = 5.68 \times 10^{-244}$, Supplementary Table 14). These three positions explained 12.9% of the variance (Fig. 4e). At position 156, residue Arg shows the largest risk effect (effect size = 0.180, $P = 8.92 \times 10^{-14}$) among the four possible allelic variants (Leu/Arg/Asp/Trp), relative to the most common residue Leu (frequency = 35.1%).

These amino acid positions mark three consecutive pockets within the HLA-B peptide-binding groove (Fig. 4c). Position 97 is located in the C-pocket and has an important role in determining the specificity of the peptide-binding groove[30,31]. Position 67 is in the B-pocket, and Met67 side chains occupy the space where larger B-pocket anchors reside in other peptide-MHC structures; its presence limits the size of potential peptide position P2 side chains[31]. Amino acid position 156 is part of the D-pocket and influences the conformation of the peptide-binding region[32]. These results are consistent with the observation that in *HLA-B*57*, the single most protective spVL-associated one-field allele (a single change at position 156 from Leu → Arg or equivalently *HLA-B*57:03* → *HLA-B*57:02*) leads to an increased repertoire of HIV-specific epitope[33,34].

Despite differences in the power to detect associations due to differences in allele frequencies (Supplementary Fig. 5), we observed generally consistent effects of individual residues across populations (Fig. 4d and Supplementary Figs. 6 and 7). There are 26 unique haplotypes defined by the amino acids at positions 67, 97 and 156 in HLA-B (Table 1 and Supplementary Table 16). When we tested for effect size heterogeneity by ancestry for each of these haplotypes (Methods), we observed only 2 of 26 haplotypes showed heterogeneity (F-test $P < 0.05/26$), possibly due to different interplay between genetic and environmental variation at the population level. These results support the concept that these positions mediate HIV-1 viral load in diverse ancestries.

To assess whether there were other independent MHC associations outside HLA-B, we conditioned on all amino acid positions in HLA-B and observed associations at HLA-A, including at position 77 in HLA-A ($P_{omnibus} = 9.10 \times 10^{-7}$, Fig. 3g,h and Supplementary Table 12), the classical *HLA* allele *HLA-A*31* ($P_{binary} = 2.45 \times 10^{-8}$) and the rs2256919 promoter SNP ($P_{binary} = 3.10 \times 10^{-16}$, Extended Data Fig. 3). These associations argue for an effect at HLA-A, but larger studies and functional studies will be necessary to define the driving effects.

We next tested for the presence of non-additive effects with respect to the three observed amino acid associations (Methods). In agreement with the previous study[14], we did not observe any single allele amino acid position showing significant departure from additivity after accounting for multiple comparisons (Supplementary Table 17).

HLA diversity.

To quantify MHC diversity, we calculated identity-by-descent (IBD) distances[35] between all individuals using 38,398 MHC single nucleotide polymorphisms (SNPs) included in the multi-ancestry HLA reference panel ($n = 21,546$) and applied principal component analysis (PCA, Methods). PCA distinguished EUR, EAS and AA as well as the admixed LAT and SAS samples (Extended Data Fig. 5 and Supplementary Fig. 8). This reflected widespread *HLA* allele frequency differences between populations (Extended Data Fig. 6). Of 130 unique common (frequency > 1%) G-group alleles, 129 demonstrated significant differences of frequencies across populations (4 degree-of-freedom Chi-square test, $P < 0.05/130$, Supplementary Figure 9). The only exception was *DQA1*01:01:01G*, which was nominally significant (unadjusted $P = 0.047$). These differences may be related to adaptive selection. For example, the *B*53:01:01G* allele is enriched in Admixed Africans (11.7% in AA versus 0.3% in others) and it has been previously associated with malaria protection[36,37]. Consistent with previous reports[9,38], we observed that *HLA-B* had the highest allelic diversity ($n = 443$) while *HLA-DQA1* had the least ($n = 17$, Extended Data Fig. 7, Supplementary Fig. 10, and Supplementary Table 18). We included the overall and population-specific frequencies of each inferred *HLA* allele at G-group resolution in Supplementary Data 4. We next tested Hardy-Weinberg equilibrium (HWE) at each of the eight loci using an exact test (Methods). In agreement with previous work[39–41], we observed that *HLA-DRB1* showed the greatest deviation from HWE, while the least deviation was for *HLA-DQA1*, which has the least allelic diversity (Supplementary Table 19). Considering five global populations individually, the null hypothesis of HWE is rejected at 3 of 8 loci in AA (*HLA-A* with $P = 0.035$; *HLA-DRB* with $P = 1.82 \times 10^{-5}$; *HLA-DPA1* with $P = 0.012$), 4 of 8 loci in EUR, 6 of 8 loci in EAS, 2 of 8 loci in LAT, and 2 of 8 loci in SAS. This strongly suggests the existence of subpopulation structure within each global population in the HLA region.

To understand the haplotype structure of HLA between pairs of HLA genes, we calculated a multiallelic LD linkage disequilibrium (LD) measurement index[42–44], ε, which is 0 when there is no LD and 1 when there is perfect LD (Extended Data Fig. 8). We observed higher ε between *DQA1*, *DQB1*, and *DRB1*, between *DPA1* and *DPB1*, and between *B* and *C* (Supplementary Fig. 11). The heterogeneity between different populations was underscored

by the presence of population-specific common (frequency >1%) high resolution long-range haplotypes (*HLA-A~C~B~DRB1~DQA1~DQB1~DPA1~DPB1*, Fig. 5, Supplementary Figs. 12–16, Supplementary Data 4, and Methods). The most common within-population haplotype was A24::DP6 (*HLA-A*24:02:01G~C*12:02:01G~B*52:01:01G~DRB1*15:02:01G~DQA1*01:03:01G~DQB1*06:01:01G~DPA1*02:01:01G~DPB1*09:01:01G*) found at a frequency of 3.61% in EAS (Supplementary Fig. 12). This haplotype is strongly associated with immune-mediated traits such as HIV[45] and ulcerative colitis[46] in Japanese individuals. The next most common haplotype was the well-described European-specific ancestral haplotype A1::DP1 or 8.1[47,48] (frequency = 2.76%, *HLA-A*01:01:01G~C*07:01:01G~B*08:01:01G~DRB1*03:01:01G~DQA1*05:01:01G~DQB1*02:01:01G~DPA1*02:01:02G~DPB1*01:01:01G*, Supplementary Fig. 13). This haplotype is associated with diverse immunopathological phenotypes in the European population, including systemic lupus erythematosus[49], myositis[50] and several other conditions[47]. We observed long-range haplotypes in admixed populations including A1::DP4 in SAS (frequency = 1.86%, Supplementary Fig. 14), A30::DP1 in AA (frequency = 1.18%, *HLA-A*30:01:01G~C*17:01:01G~B*42:01:01:G~DRB1*03:02:01G~DQA1*04:01:01G~DQB1*04:02:01G~DPA1*02:02:02G~DPB1*01:01:01G*, Supplementary Fig. 15), and A29::DP11 in LAT (frequency = 0.74%, *HLA-A*29:02:01G~C*16:01:01G~B*44*03:01:G~DRB1*07:01:01G~DQA1*02:01:01G~DQB1*02:01:01G~DPA1*02:01:01G~DPB1*11:01:01G*, Supplementary Fig. 16). These haplotypes also have associations with multiple diseases: for example, *C*06:02~B*57:01* is associated with psoriasis[51] and *A*30:01~C*17:01~B*42:01* is associated with HIV[33].

HLA selection signature.

Previous studies have suggested that recent natural selection favors African ancestry in the HLA region in admixed populations[52–55]. To test this hypothesis in our data, we obtained WGS data from a subset of individuals within two admixed populations (1,832 AA and 594 LAT, determined by the first three global principal components, Supplementary Fig. 17 and Supplementary Note). Admixed individuals have genomes that are a mosaic of different ancestries. If genetic variations or haplotypes from an ancestral population are advantageous, then they are under selection and are expected to have higher frequency than by chance. Using ELAI[56], we quantified how much the ancestry proportions differed within the MHC from the genome-wide average. In AA, we observed that the average genome-wide proportion of African ancestry was 74.5%, compared to 78.0% in the extended MHC region, corresponding to a 3.42 (95% CI: 3.35–3.49) standard deviation increase. In LAT, we observed 5.76% African ancestry genome-wide versus 16.0% in the extended MHC region, representing an increase of 4.23 (95% CI: 4.14–4.31) standard deviations (Methods). To ensure our results are robust to different local ancestry inference methods, we applied an alternative method called RFMix[57] and observed a similarly consistent MHC-specific excess of African ancestry in LAT, and also an excess in AA that was more modest (Extended Data Fig. 9).

Discussion

In our study, we demonstrated accurate imputation with a single large reference panel for HLA imputation. We have shown how this reference panel can be used to impute genetic variation at eight *HLA* classical genes accurately across a wide range of populations. Accurate imputation in multi-ancestry studies is essential for fine-mapping.

Like previous HLA imputation reference panels[11,16,58], our current work has two main limitations. First, our current implementation of the multi-ancestry reference panel is limited to G-group resolution, and amino acids outside the binding groove were taken as its best proximity (Methods). Even though we are currently unable to differentiate alleles belonging to the same G-group, we showed that the imputation accuracy is comparable inside and outside the peptide binding groove (Supplementary Table 9). The third generation sequencers (e.g., Pac-Bio SMRT[59]) will be able to provide phased, unambiguous and allele-level information at true four-field resolution. We aim to re-evaluate our panel performance, especially for accuracy outside the binding groove, when these data become more available in the future. Second, all imputation accuracy assessment is using a Beagle (v4.1) model integrated in HLA-TAPAS. We observed similar performance between Beagle (v4.1) and Minimac4 (Supplementary Fig. 18), but did not perform extensive comparison among other HLA imputation methods[10,12]. However, we note that our multi-ancestry reference panel can serve as a useful resource for method evaluation especially in a multi-ancestry setting.

Despite this limitation, we showed the utility of this approach by defining the alleles that best explain HIV-1 viral load in infected individuals. Our work implicates three amino acid positions (97, 67 and 156) in HLA-B in conferring the known protective effect of HLA class I variation on HIV-1 infection. Combining all alleles at these three positions explained 12.9% of the variance in spVL (Fig. 4e). These positions all fall within the peptide-binding groove of the respective MHC protein (Fig. 4c), indicating that variation in the amino acid content of the peptide-binding groove is the major genetic determinant of HIV control. Supported by experimental studies[34,60–62], positions highlighted in our work indicated a structural basis for the HLA association with HIV disease progression that is mediated by the conformation of the peptide within the class I binding groove. This result highlights how a study with ancestrally diverse populations can potentially point to causal variation by leveraging linkage disequilibrium differences between genetic ancestry groups.

We note that previous studies have shown that position 97 in HLA-B has the strongest association with HIV-1 spVL or case-control in African American and European populations, but highlighted different additional signals via conditional analysis (position 45, 67 in HLA-B and position 77, 95 in HLA-A in Europeans[1,14,18] and position 63, 116 and 245 in HLA-B in African Americans[18]). These signals do not explain the signals we report here; after conditioning on positions 45, 63, 116, 245 of HLA-B and 95 of HLA-A, the association of the four identified amino acids identified in this study remained significant ($P < 5 \times 10^{-8}$). In contrast, our binding groove alleles explain these other alleles; conditioning on the four amino acid positions identified in this study (positions 67, 97 and 156 in HLA-B), all previously reported positions did not pass the Bonferroni-corrected significance threshold ($P > 5 \times 10^{-8}$, Extended Data Fig. 10).

Furthermore, defining the effect sizes for *HLA* alleles across different populations is essential for defining risk of a wide-range of diseases in the clinical setting. There is increasing application of genome-wide genotyping by patients both by healthcare providers and direct-to-consumer vendors. The large effects of the MHC region for a wide-range of immune and non-immune traits makes it essential to define *HLA* allelic effect sizes in multi-ancestry studies in order to build generally applicable clinical polygenic risk scores for many diseases in diverse populations[63–66]. Resources like the one we present here will be an essential ingredient in such studies.

Methods

Ethics statement.

Study participants included in the reference panel were from the Jackson Heart Study (JHS, n = 3,027), Multi-Ethnic Study of Atherosclerosis (MESA, n = 4,620), Chronic Obstructive Pulmonary Disease Gene (COPDGene) study (n = 10,623), Estonian Biobank (EST, n = 2,244), Japan Biological Informatics Consortium (JPN (JBIC), n = 295), Biobank Japan (JPN (BBJ), n = 1,025) and 1000 Genomes Project (1KG, n = 2,504). Each study was previously approved by respective institutional review boards, including for the generation of WGS data and association with phenotypes. All participants provided written consent. Further details of cohort descriptions and phenotype definitions are described in the Supplementary Note.

All participants included in the HIV host response study were adults, and written informed consent for genetic testing was obtained from all individuals as part of the original study in which they were enrolled (Supplementary Table 10). Ethical approval was obtained from institutional review boards for each of the respective contributing centers.

HLA-TAPAS.

HLA-TAPAS (HLA-Typing At Protein for Association Studies, https://github.com/immunogenomics/HLA-TAPAS) is an HLA-focused pipeline that can handle HLA reference panel construction (*MakeReference*), HLA imputation (*SNP2HLA*), and HLA association (*HLAassoc*). It is an updated version of SNP2HLA[11] to build an imputation reference panel and perform HLA classical allele, amino acid and SNP imputation within the extended MHC region. Briefly, major updates include (1) using PLINK1.9 instead of v1.07; (2) using BEAGLE v4.1 instead of v3 for phasing and imputation; and (3) including custom R scripts for performing association and fine-mapping analysis at amino acid level in multiple ancestries. The source code is available for download (Code Availability).

We note that our current implementation of the reference panel is limited to the G-group resolution (DNA sequences that determine the exons 2 and 3 for class I and exon 2 for class II genes, Extended Data Fig. 1), and amino acid positions outside the binding groove were taken as its best approximation (Supplementary Tables 20 and 21). When converting G-group alleles to the two-field resolution, we first approximated G-group alleles to their corresponding allele at the four-field resolution based on the ordered allele list in

the distributed IPD-IMGT/HLA database[8] (version 3.32.0). We explicitly include exonic information in the HLA-TAPAS output.

Construction of a multi-ancestry HLA reference panel using whole-genome sequences.

To construct a multi-ancestry HLA imputation reference panel, we used 24,338 whole-genome sequences at different depths (Supplementary Table 1). Details of the construction using deep-coverage whole-genome sequencing are described in the Supplementary Note. Briefly, alignment and variant-calling for genomes sequenced by each cohort were performed independently. We performed local realignment and quality recalibration with the Genome Analysis Toolkit[67] (GATK; version 3.6) on Chromosome 6:25,000,000–35,000,000. We detected single nucleotide variants (SNV) and indels using GATK with HaplotypeCaller. To eliminate false-positive sites called in the MHC region, we restricted our panel to SNVs reported in 1000 Genomes Project[23] only.

We next inferred classical *HLA* alleles at G-group resolution for eight classical HLA genes (*HLA-A*, *-B*, *-C*, *-DQA1*, *-DQB1*, *-DRB1*, *-DPA1* and *-DPB1*) using a population reference graph[26,27]. To extend the reference panel versatility, we inferred amino acid variation, one-field and two-field resolution alleles from the inferred G-group alleles. To convert the G-group alleles to two-field and one-field resolution, we first approximated each G-group allele to its corresponding allele at four-field resolution based on the first allele in the ordered allele list in the distributed IPD-IMGT/HLA database[8] (version 3.32.0). We then reduced the resolution to one- and two-field based on this approximated four-field allele. After removing samples with low-coverage and failed genome-wide quality control (Supplementary Table 3), we constructed a multi-ancestry HLA imputation reference panel (n = 21,546) using the HLA-TAPAS *MakeReference* module (Methods).

Sequence-based typing of *HLA* alleles.

Genomic DNA from the 288 unrelated samples of Japanese ancestry underwent high-resolution allele typing (three-field alleles) of six classical HLA genes (*HLA-A*, *-B* and *-C* for class I; and *HLA-DRB1*, *-DQA1* and *-DPB1* for class II)[22].

The 1000 Genomes panel consists of 1,267 individuals with information on five HLA genes (*HLA-A, -B, -C, -DQB1*, and *-DRB1*) at G-group resolution among four major ancestral groups (AA, EAS, EUR and LAT)[7].

Purified DNA from the 75 donors from the GaP registry (at the Feinstein Institute for Medical Research) was sent to NHS Blood and Transplant, UK, where *HLA* typing was performed. Next-generation sequencing was done for *HLA-A*, *-B*, *-C*, *-DQB1*, *-DPB1* and *-DRB1*. PCR-sequence-specific oligonucleotide probe sequencing was performed for *HLA-DQA1* in all samples. These typing methods yielded classical allele calls for six genes at three-field (*HLA-A*, *-B*, *-C*,*-DQB1*, *-DPB1* and *-DRB1*) or G-group resolution (*HLA-DQA1*).

We obtained HLA typing of the 1,067 African American individuals included in the HIV-1 viral load study as described previously[18,68]. Briefly, seven classical HLA genes (*HLA-A, -B, -C*, *-DQA1*, *-DQB1 -DRB1* and *-DPB1*) were obtained by sequencing exons 2 and 3

and/or single-stranded conformation polymorphism PCR (i.e., at G-group resolution), and were provided at approximated two-field resolution.

A summary of all SBT of *HLA* alleles in three different cohorts (1000 Genomes, GaP registry and HIV-1) used for imputation accuracy evaluation are summarized in Supplementary Table 22.

Accuracy measure between inferred and sequence-based typing HLA genotypes.

Allelic variants at HLA genes can be typed at different resolutions: one-field HLA types specify serological activity, two-field HLA types specify the amino acids encoded by the exons of the HLA gene, and three-field types determine the full exonic sequence including synonymous variants. G-group resolution determines the sequences of the exons encoding the peptide binding groove, that is, exons 2 and 3 for class I and exon 2 for class II genes. This means many G-group alleles can map to multiple three-field and two-field *HLA* alleles.

We calculated the accuracy at each *HLA* gene by summing across the dosage of each correctly inferred *HLA* allele or amino acid across all individuals (N), and divided by the total number of observations (2*N). That is,

$$Accuracy(g) = \frac{\sum_i^N D_i\left(A_{1i,g}\right) + \sum_i^N D_i\left(A_{2i,g}\right)}{2N},$$

where *Accuracy(g)* represents the accuracy at a classical HLA gene (e.g. *HLA-B*). D_i represents the inferred dosage of an allele in individual *i*, and alleles $A_{1i,g}$ and $A_{2i,g}$ represent the true (SBT) *HLA* types for an individual *i*.

To evaluate the accuracy between the inferred and validated *HLA* types obtained from SBT at G-group resolution, we translated the highest resolution specified by the validation data to its matching G-group resolution based IMGT/HLA database (e.g. *HLA-A*01:01* → *HLA-A*01:01:01G*), and compared it to the primary output from HLA*LA or HLA-TAPAS. We also translated all G-group alleles to their matching amino acid sequences and compared them against the validation alleles; we referred to this as the amino acid level.

To evaluate imputation performance in individual classical *HLA* alleles and amino acids, we calculated the dosage r^2 correlation between imputed and SBT dosage:

$$r^2 = \frac{\left[\sum_{i=1}^N x_i y_i - \left(\sum_{i=1}^N x_i\right)\left(\sum_{i=1}^N y_i\right)/N\right]^2}{\left(\sum_{i=1}^N x_i^2 - \left(\sum_{i=1}^N x_i\right)^2/N\right)\left(\sum_{i=1}^N y_i^2 - \left(\sum_{i=1}^N y_i\right)^2/N\right)},$$

where x_i and y_i represents the inferred and SBT dosage of an allele in individual *i*. *N* represents the number of individuals.

Principal component analysis.

We performed a principal component analysis of the MHC region based on the identity-by-descent (IBD) distances between all 21,809 individuals included in the multi-ancestry reference panel. We computed the IBD distance using Beagle (Version 4.1) and averaged over 100 runs with all variants (54,474) included in the HLA reference panel. Due to uneven representation of different genetic ancestry groups (Supplementary Table 2), we applied a weighted PCA approach, where mean and standard deviation of the IBD matrix within an ancestry group are weighted inversely proportional to the sample size.

HLA haplotype frequency estimation and Hardy-Weinberg equilibrium.

We applied an expectation-maximization algorithm approach implemented in Hapl-o-Mat (v1.1)[69] to estimate HLA haplotype frequency based on eight classical *HLA* alleles inferred at G-group resolution. We estimated haplotype counts and frequencies both overall and within five continental populations (Supplementary Data 4).

To assess departure from Hardy-Weinberg Equilibrium (HWE), we used the chi-square test implemented in the BIGDAWG (v.2.3.1)[70]. We limited typing results to the first field of the nomenclature for this analysis as no ambiguity occurred on this level. We reported *P*-values obtained from the exact chi-square test on each of the eight HLA loci (*HLA*-*A*, -*B*, -*C*, -*DRB1*, -*DQA1*, -*DQB1*, -*DPA1* and -*DPB1*) in each of the five populations separately.

Local ancestry inference.

To detect local ancestry in admixed samples, we first applied ELAI[56] to chromosome 6 with 1000 Genomes Project[23] as the reference panel. We extracted 63,998 common HapMap3 SNPs between the WGS (MESA cohort) and the 1000 Genome reference panel. We used the same set of SNPs for ELAI and RFMix analysis. We applied ELAI[56] to 1,832 African Americans and 594 Latinos. For 1,832 African American individuals included in the study, we used genotypes of 99 CEU and 108 YRI in the 1000 Genome Project as reference panel, assuming admixture generation to be seven generations ago. We used two upper-layer clusters and 10 lower-layer clusters in the model. For Latinos, we selected 65 Latinos with Native American (NAT) ancestry > 75% included in the 1000 Genomes Project identified using the ADMIXTURE analysis[71] and used these individuals with high NAT, as well as CEU and YRI from 1000 Genomes as reference panels. We assumed that the admixture time was 20 generations ago. For ELAI, we used three upper-layer clusters and 15 lower-layer clusters in the model.

To address the technical concerns that local ancestry methods are biased by the high LD of the MHC region[72,73], we performed an alternative method, RFMix[57], for local ancestry inference that accounts for high LD and lack of parental reference panels. Similar deviation from genome-wide ancestry was observed using RFMix (Extended Data Fig. 10), indicating that the selection signals we observed here are robust to different inference methods.

HLA imputation in the HIV-1 viral load GWAS data in three population.

We used genome-wide genotyping data from 12,023 HIV-1 infected individuals aggregated across more than 10 different cohorts (Supplementary Table 10). The details of these

samples and quality control procedures have been described previously[14,74]. Using the HIV-1 viral load GWAS data, we extracted the genotypes of SNPs located in the extended MHC region (chr6:28–34Mb, Supplementary Table 10). We conducted genotype imputation of one-field, two-field and G-group classical *HLA* alleles and amino acid polymorphisms of the eight class I and class II HLA genes using the constructed multi-ancestry HLA imputation reference panel and the HLA-TAPAS pipeline.

After imputation, we obtained the genotypes of 640 classical alleles, 4,513 amino acid positions of the eight classical HLA genes, and 49,321 SNPs located in the extended MHC region. We excluded variants with MAF < 0.5% and imputation $r^2 < 0.5$ for all association studies. In total, we tested 51,358 variants in our association and fine-mapping study.

HLA association analysis.

For the HIV-1 viral loads of EUR, AA and LAT samples, we conducted a joint haplotype-based association analysis using a linear regression model under the assumption of additive effects of the number of HLA haplotypes for each individual. Phased haplotypes at a locus (i.e., HLA amino acid position) were constructed from the phased imputed genotypes of variants in the locus (i.e., amino acid change or SNP) and were converted to a haplotype matrix where each row is observed haplotypes (in the locus), not genotypes.

For each amino acid position, we applied a conditional haplotype analysis. We tested a multiallelic association between the HIV-1 viral load and a haplotype matrix (of the position) with covariates, including sex, study-specific PCs, and a categorical variable indicating a population. That is

$$y = \beta_0 + \sum_i^{m-1} \beta_{1i} x_i + \sum_j^C \beta_{2j} c_j,$$

where x_i is the amino acid haplotype formed by each of the m amino acid residues that occur at that position, and c_j are the covariates included in the model.

To get an omnibus *P*-value for each position, we estimated the effect of each amino acid by assessing the significance of the improvement in fit by calculating the in-model fit, compared to a null model following an F-distribution with $m - 1$ degrees of freedom. This is implemented using an ANOVA test in R as described previously[43,75]. The most frequent haplotype was excluded from a haplotype matrix as a reference haplotype for association.

For the conditional analysis, we assumed that the null model consisted of haplotypes as defined by residues at previously defined amino acid positions. The alternative model is in addition of another position with m residues. We tested whether the addition of those amino acid positions, and the creation of k additional haplotypes groups, improved on the previous set. We then assessed the significance of the improvement in the delta deviance (sum of squares) over the previous model using an F-test. We performed stepwise conditional analysis to identify additional independent signals by adjusting for the most significant amino acid position in each step until none met the significance threshold ($P = 5 \times 10^{-8}$). We

restricted analysis to haplotypes that have a minimum of 10 occurrences within HLA-B, and removed any individual with rare haplotypes for the conditional analysis.

For the exhaustive search, we tested all possible amino acid pairs and triplets for association. For each set of amino acid positions, we used the groups of residues occurring at these positions to estimate effect size and calculated for each of these models the delta deviance in risk prediction and its *P*-values compared to the null model.

Analysis of non-additive effects.

To assess non-additive associations of three reported amino acid positions (97, 67 and 156 in HLA-B), we examined disease risk of homozygotes and heterozygotes for each haplotype, using an established linear regression framework[14,76]:

$$y = \beta_0 + \beta_{1i} x_i + d_i \delta_{x_i} + \sum_j^C \beta_{2j} c_j,$$

where β_0 is the linear regression intercept, β_{1i} is the additive effect of allele i, x_i is the amino acid haplotype formed by each of the amino acid residues that occur that position, d_i represents the dominance term for each represented haplotype, $\delta_{xi} = 1$ if and only if $x_i = 1$ (heterozygous) and 0 otherwise, and c_j are the covariates included in the model (sex, study-specific PCs, and a categorical variable indicating the population).

To determine the relative non-additive effect of a specific haplotype with frequency greater than 0.5%, we assessed the change in deviance between the additive model and the non-additive model for each amino acid variant, which follows a chi-square distribution with 1 degrees of freedom. We used a significance threshold of $P < 0.05/26$ to correct for multiple tests.

Heterogeneity testing of effect sizes.

We used interaction analyses with models that included haplotype-by-ancestry (*Haplotype x Ancestry*) interaction terms. The fit of nested models was compared to a null model using the *F*-statistic with two degrees of freedom, for which the association interaction *P*-value indicated whether the inclusion of the *Haplotype x Ancestry* interaction terms improved the model fit compared to the null model that did not include the interaction terms. Interaction *P*-values for all haplotypes formed by positions 97, 67 and 156 in HLA-B are listed in Supplementary Table 16. Haplotypes that had a significant Bonferroni-corrected *Haplotype x Ancestry* interaction heterogeneity *P*-value ($P < 0.05/26$) were considered to show evidence of significant effect size heterogeneity between ancestries.

Code Availability

HLA-TAPAS, https://github.com/immunogenomics/HLA-TAPAS;

GATK version3.6, https://software.broadinstitute.org/gatk/download/archive;

HLA*PRG, https://github.com/AlexanderDilthey/MHC-PRG;

HLA*LA, https://github.com/DiltheyLab/HLA-PRG-LA;

PLINK version1.90, https://www.cog-genomics.org/plink2;

Beagle version4.1, https://faculty.washington.edu/browning/beagle/b4_1.html;

Hapl-o-Mat version1.1, https://github.com/DKMS/Hapl-o-Mat/;

BIGDAWG version2.3.6, https://cran.r-project.org/web/packages/BIGDAWG/index.html

Data Availability

All scripts and data for generating figures presented in the manuscript are available at https://github.com/immunogenomics/HLA-TAPAS. The reference panel can be accessed for imputation at the Michigan Imputation Server, https://imputationserver.sph.umich.edu. IPD-IMGT/HLA database (version 3.32.0), https://www.ebi.ac.uk/ipd/imgt/hla/. 1000 Genomes gold-standard HLA types, http://ftp.1000genomes.ebi.ac.uk/vol1/ftp/data_collections/HLA_types/.

Extended Data

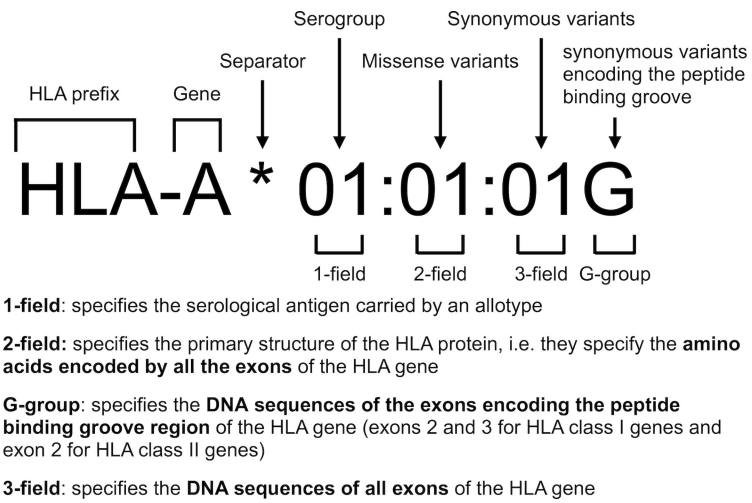

Extended Data Fig. 1. HLA nomenclature

Description of a classical HLA allele using current standard nomenclature. The first field corresponds to the serological antigen. The second field distinguishes HLA alleles that differ by one or more missense variants. The third field distinguishes HLA alleles that differ by one or more synonymous variants. The G-group distinguishes HLA alleles that differ by one or more synonymous variants within the exons that encode the peptide binding groove regions (exon 2 and 3 for HLA class I genes and exon 2 for HLA class II genes).

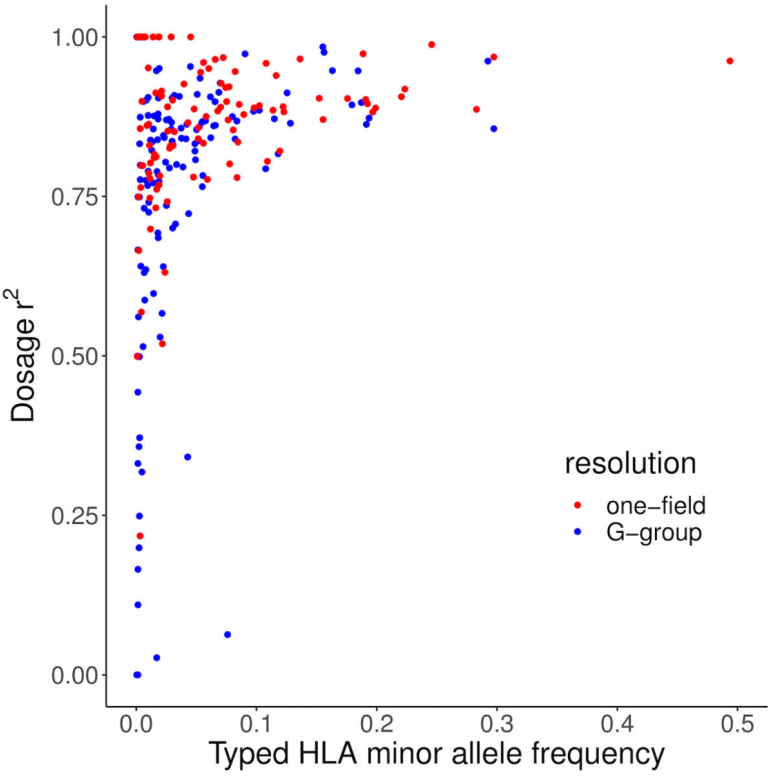

Extended Data Fig. 2. Correlation between imputed and typed dosage (dosage r^2) of classical HLA alleles in 1,067 Admixed African HIV-1 samples

The *x*-axis shows the minor allele frequency observed in the SBT dataset. Blue points show G-group *HLA* alleles. Red points show one-field *HLA* alleles.

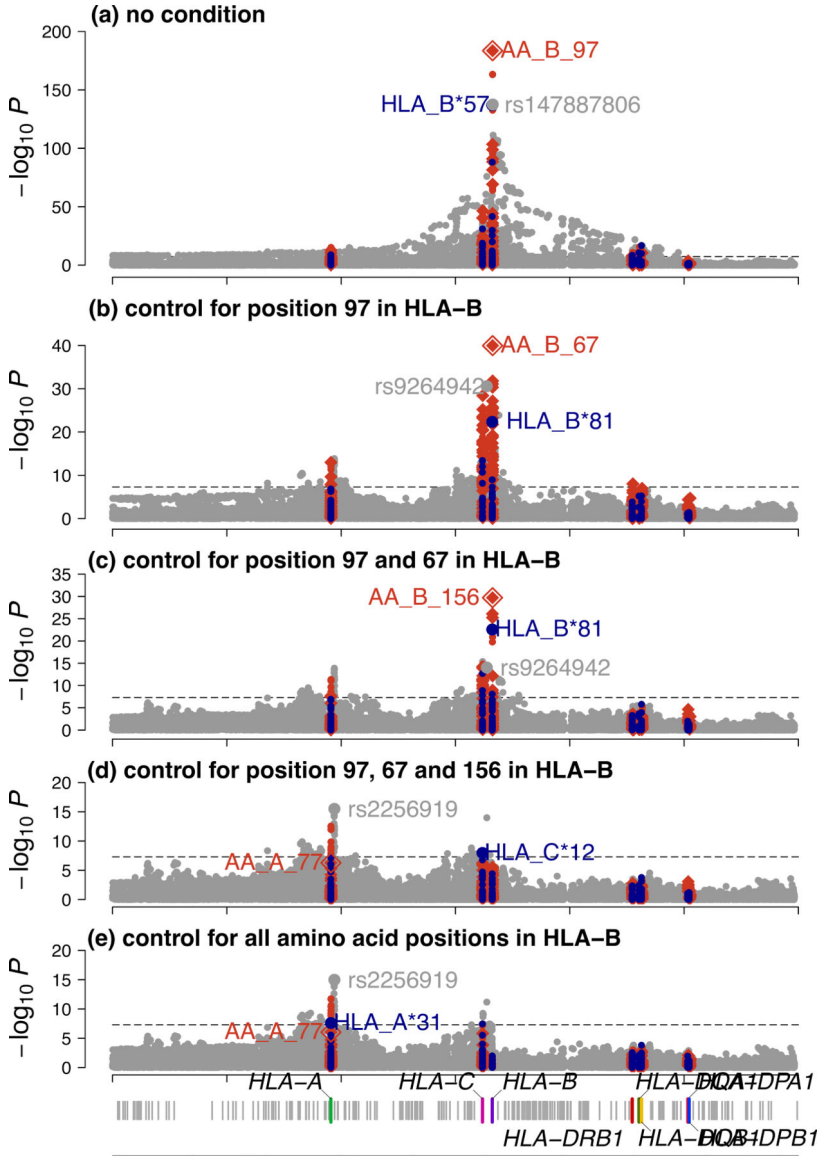

Extended Data Fig. 3. Association tests within the MHC to HIV-1 viral load

The *x*-axis shows the genomic positions of chromosome 6 (build 37), and the *y*-axis is the -$\log_{10}$ (*P*-value) obtained from two-sided regression analyses for SNPs (gray), classical HLA alleles (blue) and amino acids (red). The dashed black line indicates the genome-wide significance threshold ($P = 5 \times 10^{-8}$). For biallelic markers, results were calculated by a linear regression model including sex, cohort-specific principal components and ancestry indicator as covariates (circle). Association at amino acid positions with more than two residues was calculated using a multi-degree-of-freedom omnibus test (one-sided F-test) including the same covariates (diamond). The top associated amino acid, classical HLA allele and SNPs are annotated in the figure. **a**, Of all variants tested, the top hit maps to amino acid position 97 in HLA-B. **b**, Subsequent conditional analysis controlling for all residues at position 97 in HLA-B revealed an independent association at position 67 in HLA-B. **c**, Results conditioned on position 97 and 67 in HLA-B showed a third signal

at position 156 in HLA-B. **d**, Results conditioned on position 97, 67 and 156 in HLA-B showed position 77 in HLA-A has the strongest association signal outside HLA-B among all amino acid positions. **e**, Results conditioned on all amino acid positions in HLA-B. Notably, amino acid positions were more significant than any single SNP or classical HLA allele in each conditional analysis for the three amino acid positions in HLA-B.

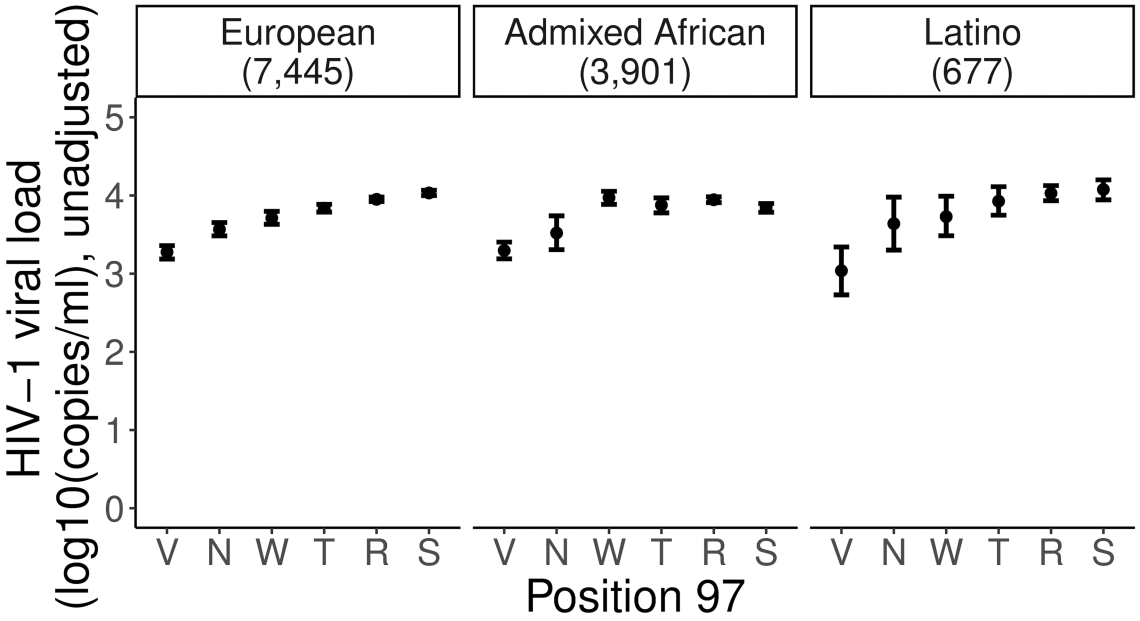

Extended Data Fig. 4. Effect on set point viral load of individual residues at position 97 in HLA-B

Mean set point viral load (spVL, RNA copies per milliliter) and its standard error of all six residues at position 97 in HLA-B in three populations independently. Data are presented as mean values ± standard errors. Residues are ranked from the most protective to the riskiest in the overall population. There are 3,901 Admixed African, 7,455 European, and 677 Latino independent samples included in the analysis.

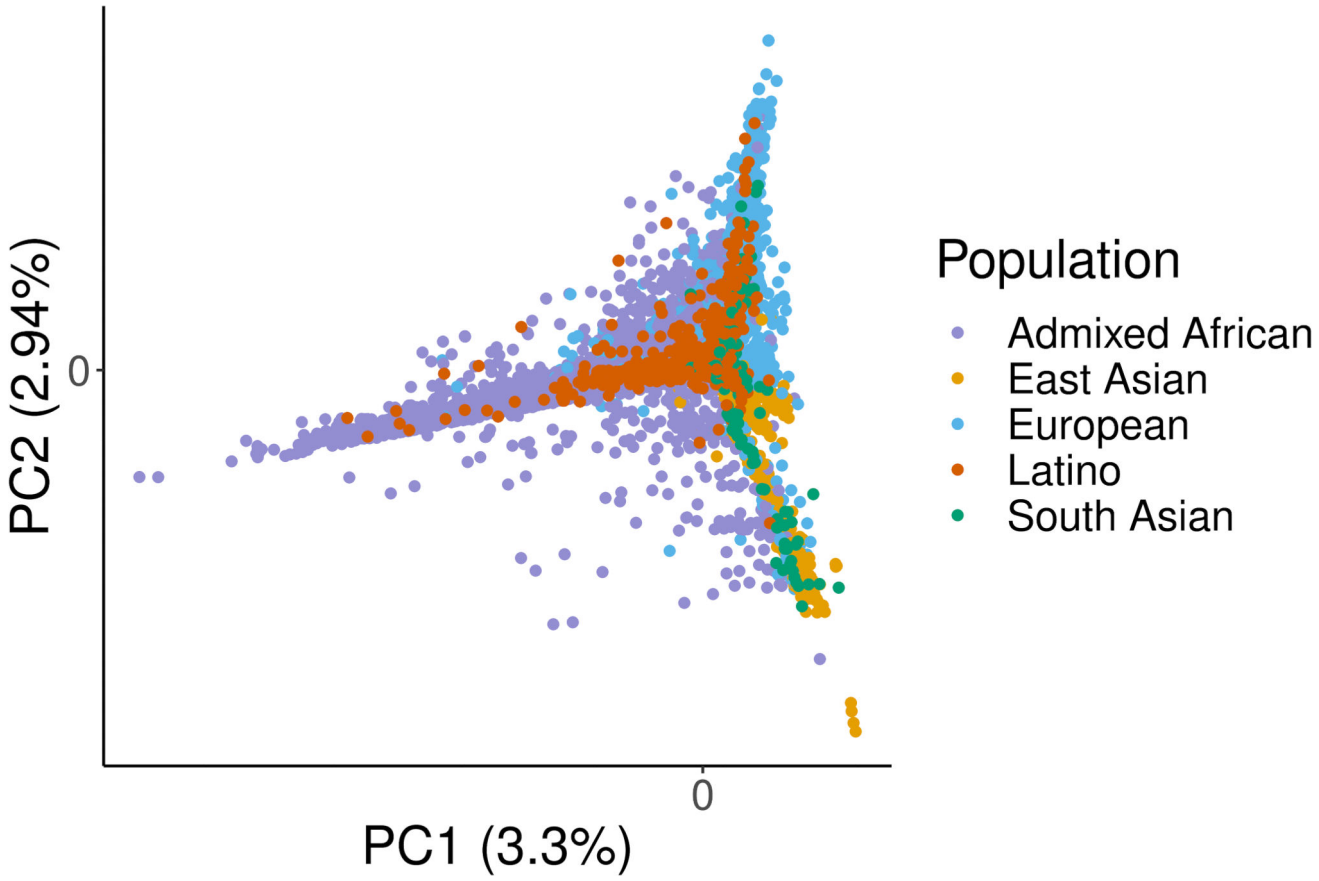

Extended Data Fig. 5. Global diversity of the MHC region

Principal component analysis of the pairwise IBD distance between 21,546 samples using MHC region markers. The first two principal components show separation of continental groups.

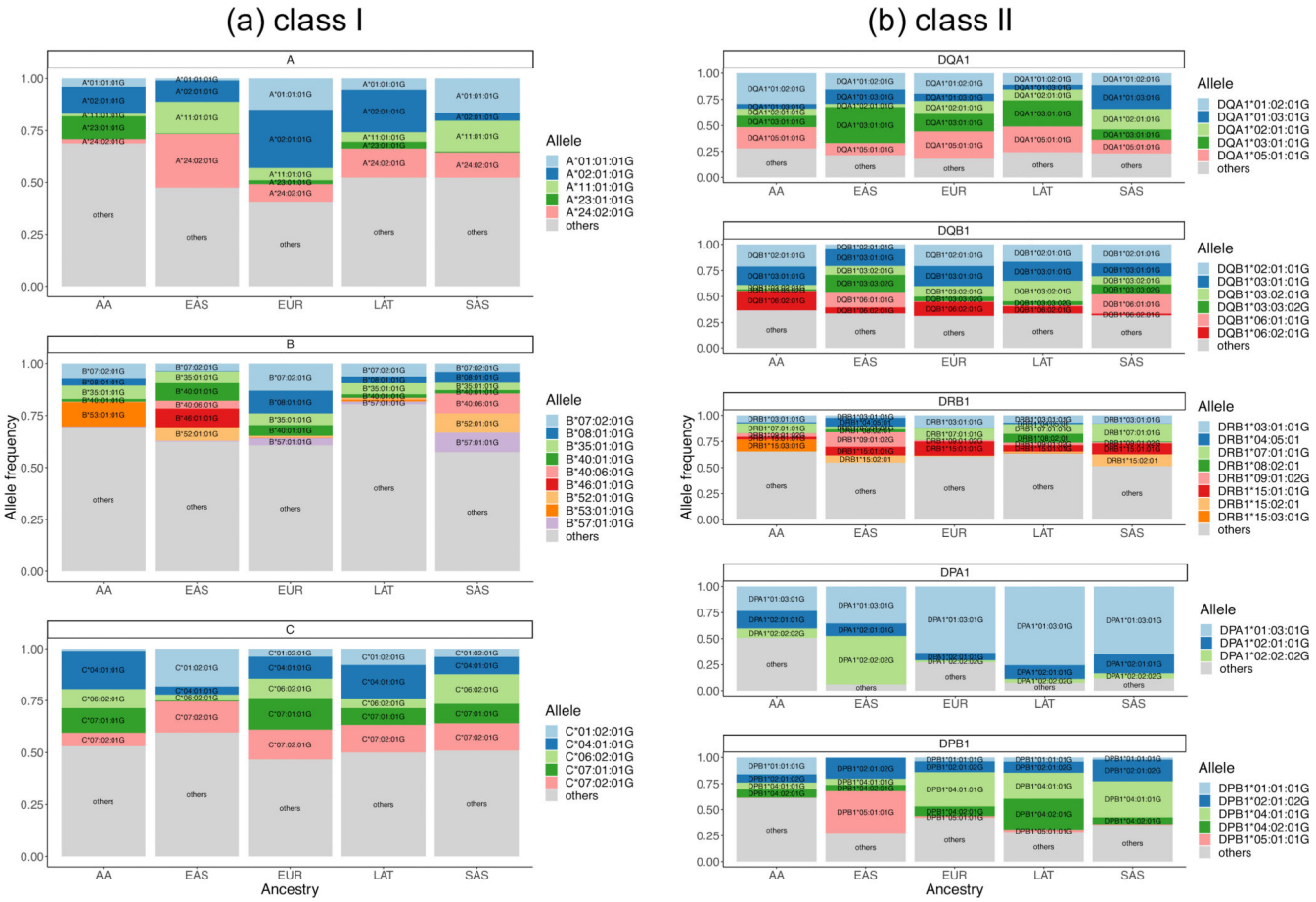

Extended Data Fig. 6. Diversity of eight classical HLA genes in the constructed multi-ancestry MHC reference panel

Each gene is stratified by six populations (AA, Admixed African; EAS, East Asian; EUR, European; LAT, Latino; SAS, South Asian). The top two most common alleles within each classical gene of each population are plotted across all panels. Alleles that have frequencies greater than 1% are also labelled in the bar plots. **a**, Class I genes. **b**, Class II genes.

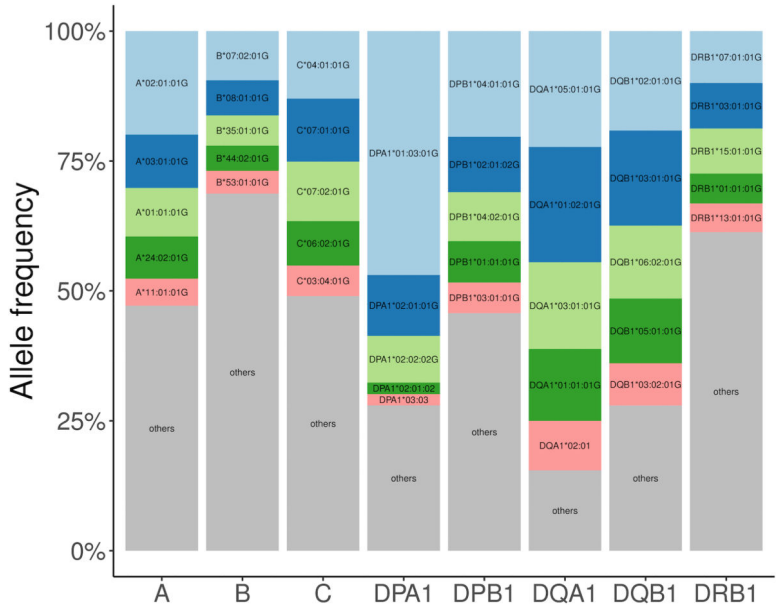

Extended Data Fig. 7. Allele diversity of eight classical HLA genes in global populations

For each gene, the top five most frequent alleles across all populations are shown (light blue, most frequent; dark blue, second frequent; light green, third frequent; dark green, fourth frequent; red, fifth frequent; gray, all other alleles).

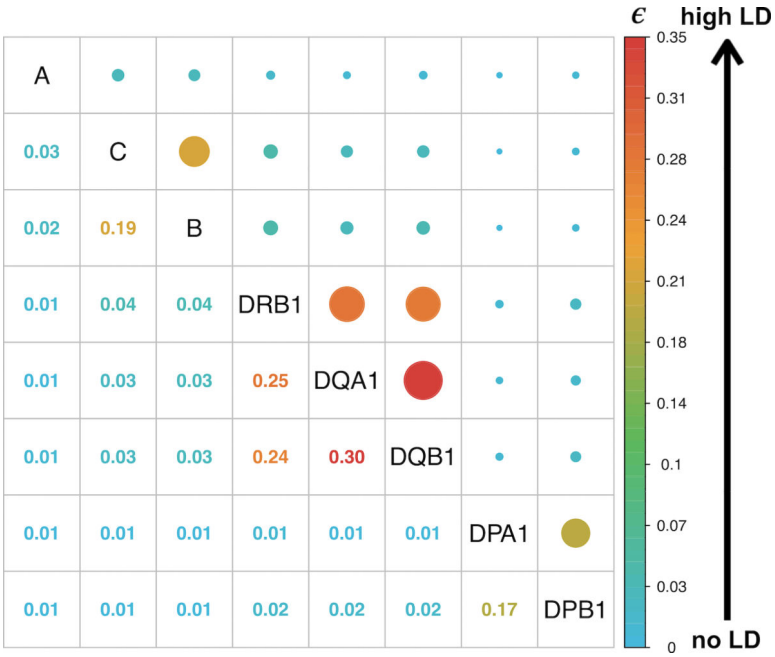

Extended Data Fig. 8. Pairwise normalized entropy (ε) among all population groups

The normalized entropy (ε) measures the difference of the haplotype frequency distribution for linkage disequilibrium and linkage equilibrium, and takes values between 0 (no LD) to 1 (perfect LD).

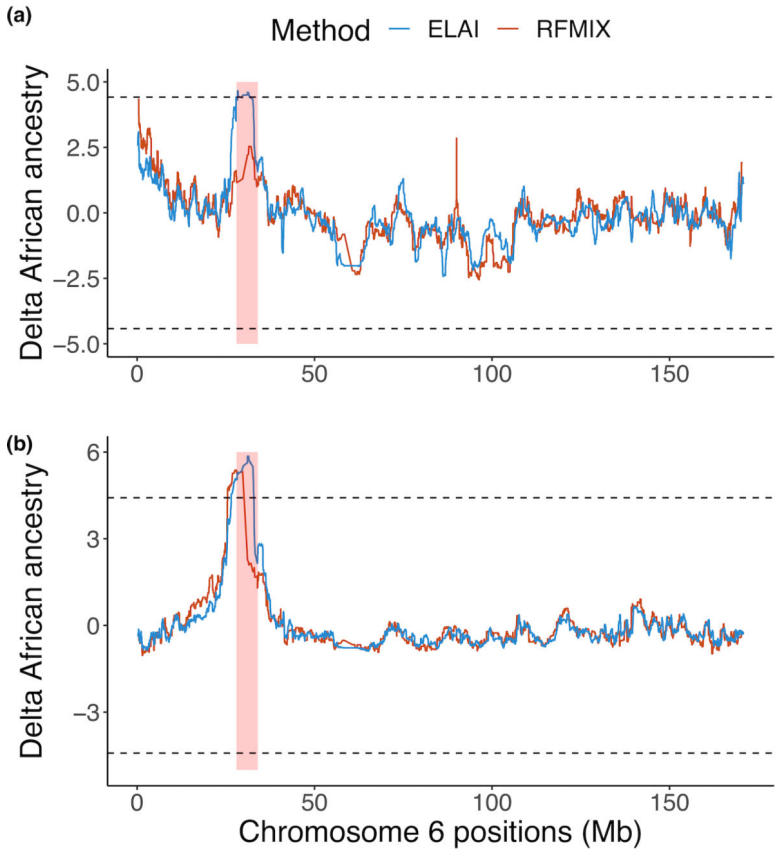

Extended Data Fig. 9. Deviation from average genome-wide ancestry in Admixed African and Latino populations

a,**b**, The *x*-axis is the genomic position of chromosome 6. The *y*-axis shows the local African ancestry deviation measure inferred at a given position for Admixed Africans (**a**) and Latinos (**b**). The MHC region (chr6:28Mb-34Mb) is highlighted in red shading. Local ancestries were estimated using RFMix (red) and ELAI (blue). The ancestry deviation measure is the difference between African ancestry at a given genomic position with respect to the genome-wide average estimated by ADMIXTURE with K = 3, normalized by the standard deviation of the ancestry estimate. The dashed line indicates the genome-wide significance threshold at ±4.42 standard deviation of the ancestry estimate deviated from the genome-wide average.

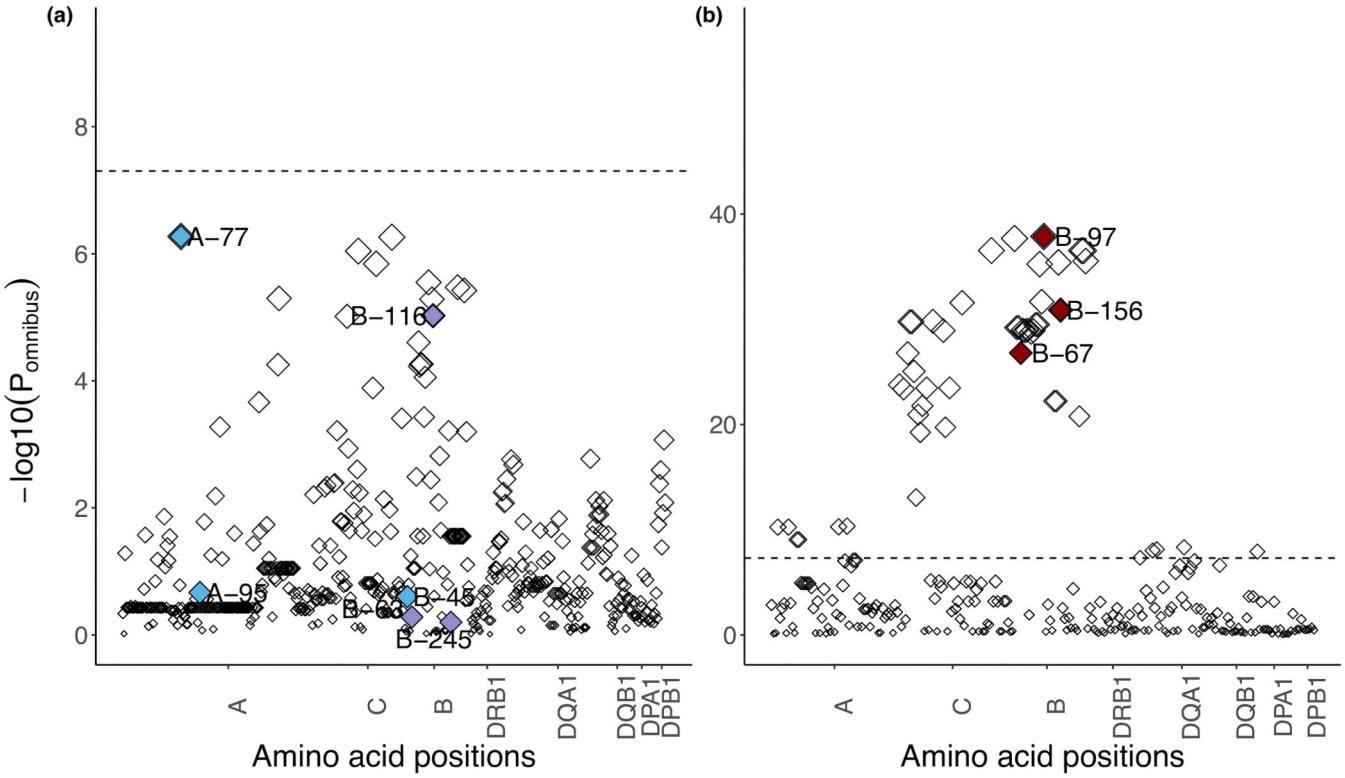

Extended Data Fig. 10. Conditional analysis of other previously reported independently associated amino acid positions

a,**b**, Manhattan plots of amino acid positions in the six classical HLA genes. Each point shows a single amino acid position and its omnibus *P*-value after controlling for independent positions that are associated with spVL in this study (position 97, 67 and 156 in HLA-B) (**a**) and independent positions that are only reported in previous studies[14,18] and not in the presented work (position 45, 63 and 116 in HLA-B and position 77, 95 in HLA-A) (**b**). Independently associated amino acid positions that are only reported in the European population[14] are shown in blue. Independently associated amino acid positions that are only reported in the African American population[18] are shown in purple. Independently associated amino acid positions identified in this study are shown in red.

Supplementary Material

Refer to Web version on PubMed Central for supplementary material.

Acknowledgements

The study was supported by the National Institutes of Health (NIH) TB Research Unit Network, Grant U19 AI111224-01.

We thank Cristen Willer, Brett Vanderwerff and Bethany Klunder from the University of Michigan for help facilitating getting the constructed reference panel on the Michigan Imputation Server.

The views expressed in this manuscript are those of the authors and do not necessarily represent the views of the National Heart, Lung, and Blood Institute; the National Institutes of Health; or the U.S. Department of Health and Human Services.

The Genotype and Phenotype (GaP) Registry at The Feinstein Institute for Medical Research provided fresh, de-identified human plasma; blood was collected from control subjects under an IRB-approved protocol (IRB# 09-081) and processed to isolate plasma. The GaP is a sub-protocol of the Tissue Donation Program (TDP) at Northwell Health and a national resource for genotype-phenotype studies. https://www.feinsteininstitute.org/robert-s-boas-center-for-genomics-and-human-genetics/gap-registry/

For some HIV cohort participants, DNA and data collection was supported by NIH/NIAID AIDS Clinical Trial Group (ACTG) grants UM1 AI068634, UM1 AI068636 and UM1 AI106701, and ACTG clinical research site grants A1069412, A1069423, A1069424, A1069503, AI025859, AI025868, AI027658, AI027661, AI027666, AI027675, AI032782, AI034853, AI038858, AI045008, AI046370, AI046376, AI050409, AI050410, AI050410, AI058740, AI060354, AI068636, AI069412, AI069415, AI069418, AI069419, AI069423, AI069424, AI069428, AI069432, AI069432, AI069434, AI069439, AI069447, AI069450, AI069452, AI069465, AI069467, AI069470, AI069471, AI069472, AI069474, AI069477, AI069481, AI069484, AI069494, AI069495, AI069496, AI069501, AI069501, AI069502, AI069503, AI069511, AI069513, AI069532, AI069534, AI069556, AI072626, AI073961, RR000046, RR000425, RR023561, RR024156, RR024160, RR024996, RR025008, RR025747, RR025777, RR025780, TR000004, TR000058, TR000124, TR000170, TR000439, TR000445, TR000457, TR001079, TR001082, TR001111, and TR024160.

Molecular data for the Trans-Omics in Precision Medicine (TOPMed) program was supported by the National Heart, Lung and Blood Institute (NHLBI). See the TOPMed Omics Support Table (Supplementary Table 23) for study specific omics support information. Core support including centralized genomic read mapping and genotype calling, along with variant quality metrics and filtering were provided by the TOPMed Informatics Research Center (3R01HL-117626-02S1; contract HHSN268201800002I). Core support including phenotype harmonization, data management, sample-identity QC, and general program coordination were provided by the TOPMed Data Coordinating Center (R01HL-120393; U01HL-120393; contract HHSN268201800001I). We gratefully acknowledge the studies and participants who provided biological samples and data for TOPMed.

The COPDGene project was supported by Award Number U01 HL089897 and Award Number U01 HL089856 from the National Heart, Lung, and Blood Institute. The content is solely the responsibility of the authors and does not necessarily represent the official views of the National Heart, Lung, and Blood Institute or the National Institutes of Health. The COPDGene project is also supported by the COPD Foundation through contributions made to an Industry Advisory Board comprised of AstraZeneca, Boehringer Ingelheim, GlaxoSmithKline, Novartis, Pfizer, Siemens and Sunovion. A full listing of COPDGene investigators can be found at http://www.copdgene.org/directory.

The Jackson Heart Study (JHS) is supported and conducted in collaboration with Jackson State University (HHSN268201800013I), Tougaloo College (HHSN268201800014I), the Mississippi State Department of Health (HHSN268201800015I) and the University of Mississippi Medical Center (HHSN268201800010I, HHSN268201800011I and HHSN268201800012I) contracts from the National Heart, Lung, and Blood Institute (NHLBI) and the National Institute on Minority Health and Health Disparities (NIMHD). The authors also wish to thank the staffs and participants of the JHS.

MESA and the MESA SHARe project are conducted and supported by the National Heart, Lung, and Blood Institute (NHLBI) in collaboration with MESA investigators. Support for MESA is provided by contracts 75N92020D00001, HHSN268201500003I, N01-HC-95159, 75N92020D00005, N01-HC-95160, 75N92020D00002, N01-HC-95161, 75N92020D00003, N01-HC-95162, 75N92020D00006, N01-HC-95163, 75N92020D00004, N01-HC-95164, 75N92020D00007, N01-HC-95165, N01-HC-95166, N01-HC-95167, N01-HC-95168, N01-HC-95169, UL1-TR-000040, UL1-TR-001079, UL1-TR-001420. MESA Family is conducted and supported by the National Heart, Lung, and Blood Institute (NHLBI) in collaboration with MESA investigators. Support is provided by grants and contracts R01HL071051, R01HL071205, R01HL071250, R01HL071251, R01HL071258, R01HL071259, by the National Center for Research Resources, Grant UL1RR033176. The provision of genotyping data was supported in part by the National Center for Advancing Translational Sciences, CTSI grant UL1TR001881, and the National Institute of Diabetes and Digestive and Kidney Disease Diabetes Research Center (DRC) grant DK063491 to the Southern California Diabetes Endocrinology Research Center. This project has been funded in whole or in part with federal funds from the Frederick National Laboratory for Cancer Research, under Contract No. HHSN261200800001E. The content of this publication does not necessarily reflect the views or policies of the Department of Health and Human Services, nor does mention of trade names, commercial products, or organizations imply endorsement by the U.S. Government. This Research was supported in part by the Intramural Research Program of the NIH, Frederick National Lab, Center for Cancer Research.

D.H.S. was supported by R01 HL92301, R01 HL67348, R01 NS058700, R01 AR48797, R01 DK071891, R01 AG058921, the General Clinical Research Center of the Wake Forest University School of Medicine (M01 RR07122, F32 HL085989), the American Diabetes Association, and a pilot grant from the Claude Pepper Older Americans Independence Center of Wake Forest University Health Sciences (P60 AG10484). A.M. is supported by Gentransmed grant 2014-2020.4.01.15-0012. D.W.H. is supported by NIH grants AI110527, AI077505, TR000445, AI069439, and AI110527. J.T.E. and P.E.S. were supported by NIH/NIAMS R01 AR042742, R01 AR050511,

and R01 AR063611. Y.O. was supported by the Japan Society for the Promotion of Science (JSPS) KAKENHI (19H01021, 20K21834), and AMED (JP20km0405211, JP20ek0109413, JP20ek0410075, JP20gm4010006, and JP20km0405217), Takeda Science Foundation, and Bioinformatics Initiative of Osaka University Graduate School of Medicine, Osaka University.

Competing Interests

M.H.C. has received consulting or speaking fees from Illumina and AstraZeneca, and grant support from GSK and Bayer. The remaining authors declare no competing interests.

References

1. International HIV Controllers Study et al. The major genetic determinants of HIV-1 control affect HLA class I peptide presentation. Science 330, 1551–1557 (2010). [PubMed: 21051598]
2. Raychaudhuri S et al. Five amino acids in three HLA proteins explain most of the association between MHC and seropositive rheumatoid arthritis. Nat. Genet. 44, 291–296 (2012). [PubMed: 22286218]
3. Evans DM et al. Interaction between ERAP1 and HLA-B27 in ankylosing spondylitis implicates peptide handling in the mechanism for HLA-B27 in disease susceptibility. Nat. Genet. 43, 761–767 (2011). [PubMed: 21743469]
4. Snyder A et al. Genetic basis for clinical response to CTLA-4 blockade in melanoma. N. Engl. J. Med. 371, 2189–2199 (2014). [PubMed: 25409260]
5. Buniello A et al. The NHGRI-EBI GWAS Catalog of published genome-wide association studies, targeted arrays and summary statistics 2019. Nucleic Acids Res. 47, D1005–D1012 (2019). [PubMed: 30445434]
6. Horton R et al. Gene map of the extended human MHC. Nat. Rev. Genet. 5, 889–899 (2004). [PubMed: 15573121]
7. Gourraud P-A et al. HLA diversity in the 1000 genomes dataset. PLoS One 9, e97282 (2014). [PubMed: 24988075]
8. Robinson J et al. IPD-IMGT/HLA Database. Nucleic Acids Res. 48, D948–D955 (2020). [PubMed: 31667505]
9. Gonzalez-Galarza FF et al. Allele frequency net database (AFND) 2020 update: gold-standard data classification, open access genotype data and new query tools. Nucleic Acids Res. 48, D783–D788 (2020). [PubMed: 31722398]
10. Dilthey AT, Moutsianas L, Leslie S & McVean G HLA*IMP—an integrated framework for imputing classical HLA alleles from SNP genotypes. Bioinformatics 27, 968–972 (2011). [PubMed: 21300701]
11. Jia X et al. Imputing amino acid polymorphisms in human leukocyte antigens. PLoS One 8, e64683 (2013). [PubMed: 23762245]
12. Zheng X et al. HIBAG—HLA genotype imputation with attribute bagging. Pharmacogenomics J. 14, 192–200 (2014). [PubMed: 23712092]
13. Hu X et al. Additive and interaction effects at three amino acid positions in HLA-DQ and HLA-DR molecules drive type 1 diabetes risk. Nat. Genet. 47, 898–905 (2015). [PubMed: 26168013]
14. McLaren PJ et al. Polymorphisms of large effect explain the majority of the host genetic contribution to variation of HIV-1 virus load. Proc. Natl. Acad. Sci. U. S. A. 112, 14658–14663 (2015). [PubMed: 26553974]
15. Tian C et al. Genome-wide association and HLA region fine-mapping studies identify susceptibility loci for multiple common infections. Nat. Commun. 8, 599 (2017). [PubMed: 28928442]
16. Onengut-Gumuscu S et al. Type 1 diabetes risk in African-ancestry participants and utility of an ancestry-specific genetic risk score. Diabetes Care 42, 406–415 (2019). [PubMed: 30659077]
17. HIV/AIDS. https://www.who.int/news-room/fact-sheets/detail/hiv-aids.
18. McLaren PJ et al. Fine-mapping classical HLA variation associated with durable host control of HIV-1 infection in African Americans. Hum. Mol. Genet. 21, 4334–4347 (2012). [PubMed: 22718199]

19. Taliun D et al. Sequencing of 53,831 diverse genomes from the NHLBI TOPMed Program. Nature 590, 290–299 (2021). [PubMed: 33568819]
20. Okada Y et al. Deep whole-genome sequencing reveals recent selection signatures linked to evolution and disease risk of Japanese. Nat. Commun. 9, 1631 (2018). [PubMed: 29691385]
21. Mitt M et al. Improved imputation accuracy of rare and low-frequency variants using population-specific high-coverage WGS-based imputation reference panel. Eur. J. Hum. Genet. 25, 869–876 (2017). [PubMed: 28401899]
22. Hirata J et al. Genetic and phenotypic landscape of the major histocompatibilty complex region in the Japanese population. Nat. Genet. 51, 470–480 (2019). [PubMed: 30692682]
23. 1000 Genomes Project Consortium et al. A global reference for human genetic variation. Nature 526, 68–74 (2015). [PubMed: 26432245]
24. Nelis M et al. Genetic structure of Europeans: a view from the north-east. PLoS One 4, (2009).
25. Dilthey A, Cox C, Iqbal Z, Nelson MR & McVean G Improved genome inference in the MHC using a population reference graph. Nat. Genet. 47, 682–688 (2015). [PubMed: 25915597]
26. Dilthey AT et al. High-accuracy HLA type inference from whole-genome sequencing data using population reference graphs. PLoS Comput. Biol. 12, e1005151 (2016). [PubMed: 27792722]
27. Dilthey AT et al. HLA*LA-HLA typing from linearly projected graph alignments. Bioinformatics 35, 4394–4396 (2019). [PubMed: 30942877]
28. Mellors JW et al. Quantitation of HIV-1 RNA in plasma predicts outcome after seroconversion. Ann. Intern. Med. 122, 573–579 (1995). [PubMed: 7887550]
29. Bartha I et al. Estimating the respective contributions of human and viral genetic variation to HIV control. PLoS Comput. Biol. 13, e1005339 (2017). [PubMed: 28182649]
30. Blanco-Gelaz MA et al. The amino acid at position 97 is involved in folding and surface expression of HLA-B27. Int. Immunol. 18, 211–220 (2006). [PubMed: 16361312]
31. Stewart-Jones GBE et al. Structures of three HIV-1 HLA-B*5703-peptide complexes and identification of related HLAs potentially associated with long-term nonprogression. J. Immunol. 175, 2459–2468 (2005). [PubMed: 16081817]
32. Archbold JK et al. Natural micropolymorphism in human leukocyte antigens provides a basis for genetic control of antigen recognition. J. Exp. Med. 206, 209–219 (2009). [PubMed: 19139173]
33. Kløverpris HN et al. HIV control through a single nucleotide on the HLA-B locus. J. Virol. 86, 11493–11500 (2012). [PubMed: 22896606]
34. Gaiha GD et al. Structural topology defines protective CD8+ T cell epitopes in the HIV proteome. Science 364, 480–484 (2019). [PubMed: 31048489]
35. Browning BL & Browning SR A fast, powerful method for detecting identity by descent. Am. J. Hum. Genet. 88, 173–182 (2011). [PubMed: 21310274]
36. Hill AV et al. Common west African HLA antigens are associated with protection from severe malaria. Nature 352, 595–600 (1991). [PubMed: 1865923]
37. Sanchez-Mazas A et al. The HLA-B landscape of Africa: Signatures of pathogen-driven selection and molecular identification of candidate alleles to malaria protection. Mol. Ecol. 26, 6238–6252 (2017). [PubMed: 28950417]
38. Maiers M, Gragert L & Klitz W High-resolution HLA alleles and haplotypes in the United States population. Hum. Immunol. 68, 779–788 (2007). [PubMed: 17869653]
39. Chen JJ et al. Hardy-Weinberg testing for HLA class II (DRB1, DQA1, DQB1, AND DPB1) loci in 26 human ethnic groups. Tissue Antigens 54, 533–542 (1999). [PubMed: 10674966]
40. Tshabalala M et al. Human Leukocyte Antigen-A, B, C, DRB1, and DQB1 allele and haplotype frequencies in a subset of 237 donors in the South African Bone Marrow Registry. J. Immunol. Res. 2018, 2031571 (2018). [PubMed: 29850621]
41. Hagenlocher Y et al. 6-Locus HLA allele and haplotype frequencies in a population of 1075 Russians from Karelia. Hum. Immunol. 80, 95–96 (2019). [PubMed: 30391501]
42. Nothnagel M, Fürst R & Rohde K Entropy as a measure for linkage disequilibrium over multilocus haplotype blocks. Hum. Hered. 54, 186–198 (2002). [PubMed: 12771551]

43. Okada Y et al. Construction of a population-specific HLA imputation reference panel and its application to Graves' disease risk in Japanese. Nat. Genet. 47, 798–802 (2015). [PubMed: 26029868]
44. Okada Y eLD: entropy-based linkage disequilibrium index between multiallelic sites. Hum. Genome Var. 5, 29 (2018). [PubMed: 30374405]
45. Chikata T et al. Host-specific adaptation of HIV-1 subtype B in the Japanese population. J. Virol. 88, 4764–4775 (2014). [PubMed: 24522911]
46. Nomura E et al. Mapping of a disease susceptibility locus in chromosome 6p in Japanese patients with ulcerative colitis. Genes Immun. 5, 477–483 (2004). [PubMed: 15215890]
47. Price P et al. The genetic basis for the association of the 8.1 ancestral haplotype (A1, B8, DR3) with multiple immunopathological diseases. Immunol. Rev. 167, 257–274 (1999). [PubMed: 10319267]
48. Horton R et al. Variation analysis and gene annotation of eight MHC haplotypes: the MHC Haplotype Project. Immunogenetics 60, 1–18 (2008). [PubMed: 18193213]
49. Graham RR et al. Visualizing human leukocyte antigen class II risk haplotypes in human systemic lupus erythematosus. Am. J. Hum. Genet. 71, 543–553 (2002). [PubMed: 12145745]
50. Miller FW et al. Genome-wide association study identifies HLA 8.1 ancestral haplotype alleles as major genetic risk factors for myositis phenotypes. Genes Immun. 16, 470–480 (2015). [PubMed: 26291516]
51. Haapasalo K et al. The psoriasis risk allele HLA-C*06:02 shows evidence of association with chronic or recurrent Streptococcal tonsillitis. Infect. Immun. 86, e00304–18 (2018). [PubMed: 30037793]
52. Salter-Townshend M & Myers S Fine-scale inference of ancestry segments without prior knowledge of admixing groups. Genetics 212, 869–889 (2019). [PubMed: 31123038]
53. Zhou Q, Zhao L & Guan Y Strong Selection at MHC in Mexicans since Admixture. PLoS Genet. 12, e1005847 (2016). [PubMed: 26863142]
54. Meyer D, C Aguiar VR, Bitarello BD, C Brandt DY & Nunes K A genomic perspective on HLA evolution. Immunogenetics 70, 5–27 (2018). [PubMed: 28687858]
55. Norris ET et al. Admixture-enabled selection for rapid adaptive evolution in the Americas. Genome Biol. 21, 29 (2020). [PubMed: 32028992]
56. Guan Y Detecting structure of haplotypes and local ancestry. Genetics 196, 625–642 (2014). [PubMed: 24388880]
57. Maples BK, Gravel S, Kenny EE & Bustamante CD RFMix: a discriminative modeling approach for rapid and robust local-ancestry inference. Am. J. Hum. Genet. 93, 278–288 (2013). [PubMed: 23910464]
58. Degenhardt F et al. Construction and benchmarking of a multi-ethnic reference panel for the imputation of HLA class I and II alleles. Hum. Mol. Genet. 28, 2078–2092 (2019). [PubMed: 30590525]
59. Ambardar S & Gowda M High-resolution full-length HLA typing method using third generation (Pac-Bio SMRT) sequencing technology. Methods Mol. Biol. 1802, 135–153 (2018). [PubMed: 29858806]
60. Macdonald WA et al. A naturally selected dimorphism within the HLA-B44 supertype alters class I structure, peptide repertoire, and T cell recognition. J. Exp. Med. 198, 679–691 (2003). [PubMed: 12939341]
61. Kloverpris HN et al. HLA-B*57 micropolymorphism shapes HLA allele-specific epitope immunogenicity, selection pressure, and HIV immune control. J. Virol. 86, 919–929 (2012). [PubMed: 22090105]
62. Carrington M & Walker BD Immunogenetics of spontaneous control of HIV. Annu. Rev. Med. 63, 131–145 (2012). [PubMed: 22248321]
63. Khera AV et al. Genome-wide polygenic scores for common diseases identify individuals with risk equivalent to monogenic mutations. Nat. Genet. 50, 1219–1224 (2018). [PubMed: 30104762]
64. Khera AV et al. Polygenic prediction of weight and obesity trajectories from birth to adulthood. Cell 177, 587–596.e9 (2019). [PubMed: 31002795]

65. Torkamani A & Topol E Polygenic risk scores expand to obesity. Cell 177, 518–520 (2019). [PubMed: 31002792]

66. Martin AR et al. Clinical use of current polygenic risk scores may exacerbate health disparities. Nat. Genet. 51, 584–591 (2019). [PubMed: 30926966]

67. Van der Auwera GA et al. From FastQ data to high confidence variant calls: the Genome Analysis Toolkit best practices pipeline. Curr. Protoc. Bioinformatics 43, 11.10.1–33 (2013). [PubMed: 25431634]

68. Julg B et al. Possession of HLA class II DRB1*1303 associates with reduced viral loads in chronic HIV-1 clade C and B infection. J. Infect. Dis. 203, 803–809 (2011). [PubMed: 21257739]

69. Schäfer C, Schmidt AH & Sauter J Hapl-o-Mat: open-source software for HLA haplotype frequency estimation from ambiguous and heterogeneous data. BMC Bioinformatics 18, 284 (2017). [PubMed: 28558647]

70. Pappas DJ, Marin W, Hollenbach JA & Mack SJ Bridging ImmunoGenomic Data Analysis Workflow Gaps (BIGDAWG): An integrated case-control analysis pipeline. Hum. Immunol. 77, 283–287 (2016). [PubMed: 26708359]

71. Alexander DH, Novembre J & Lange K Fast model-based estimation of ancestry in unrelated individuals. Genome Res. 19, 1655–1664 (2009). [PubMed: 19648217]

72. Price AL et al. Long-range LD can confound genome scans in admixed populations. Am. J. Hum. Genet. 83, 132–135 (2008). [PubMed: 18606306]

73. Pasaniuc B et al. Analysis of Latino populations from GALA and MEC studies reveals genomic loci with biased local ancestry estimation. Bioinformatics 29, 1407–1415 (2013). [PubMed: 23572411]

74. McLaren PJ et al. Association study of common genetic variants and HIV-1 acquisition in 6,300 infected cases and 7,200 controls. PLoS Pathog. 9, e1003515 (2013). [PubMed: 23935489]

75. Okada Y et al. Contribution of a non-classical HLA gene, HLA-DOA, to the risk of rheumatoid arthritis. Am. J. Hum. Genet. 99, 366–374 (2016). [PubMed: 27486778]

76. Lenz TL et al. Widespread non-additive and interaction effects within HLA loci modulate the risk of autoimmune diseases. Nat. Genet. 47, 1085–1090 (2015). [PubMed: 26258845]

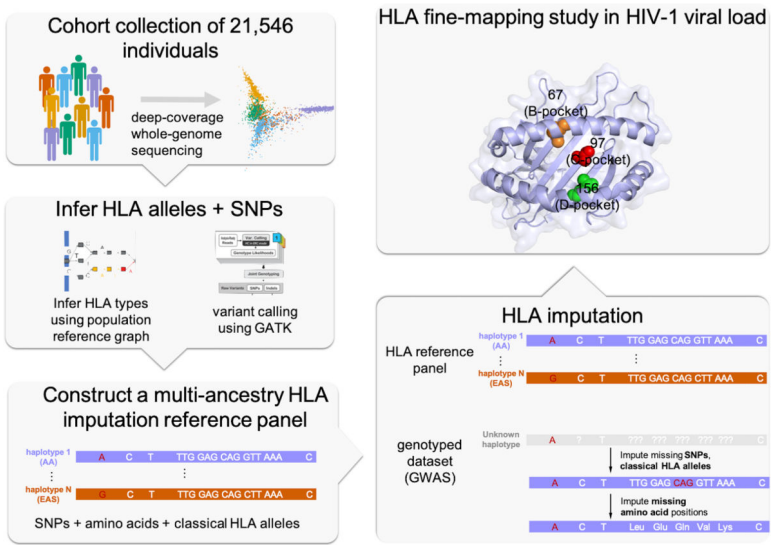

Figure 1 |. A schematic showing the overall study design.

We used whole-genome sequences of 21,546 individuals from five global populations to construct an HLA imputation reference panel. We then performed HLA imputation and fine-mapping in HIV-1 viral load jointly in three populations.

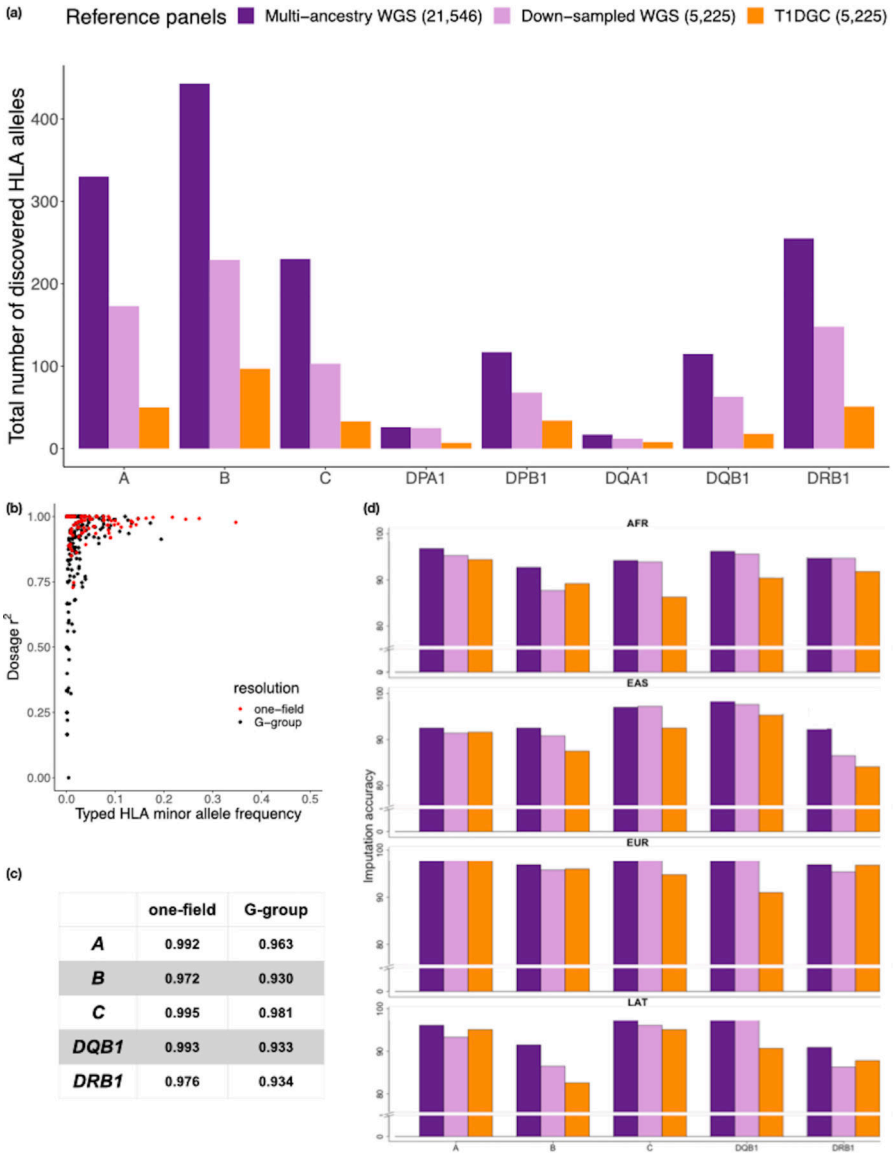

	one-field	G-group
A	0.992	0.963
B	0.972	0.930
C	0.995	0.981
DQB1	0.993	0.933
DRB1	0.976	0.934

Figure 2 |. The multi-ancestry HLA reference panel shows improvement in allele diversity and imputation accuracy.

a, The number of *HLA* alleles at the two-field resolution included in the multi-ancestry HLA reference panel (n = 21,546) compared to the European only Type 1 Diabetes Genetics Consortium (T1DGC) panel (n = 5,225) as well as a subset of the multi-ancestry HLA panel down-sampled to the same size as T1DGC. **b**, The correlation between imputed and typed dosages of classical *HLA* alleles using the multi-ancestry HLA reference panel at one-filed (red) and G-group resolution (black) of 955 individuals with SBT HLA typing data from the 1000 Genomes project. **c**, The imputation accuracy for five classical HLA genes at one-field, two-field and G-group resolution. **d**, The imputation accuracy at G-group resolution of the 1000 Genomes individuals stratified by four diverse ancestries when using three different imputation reference panels as described in **a**.

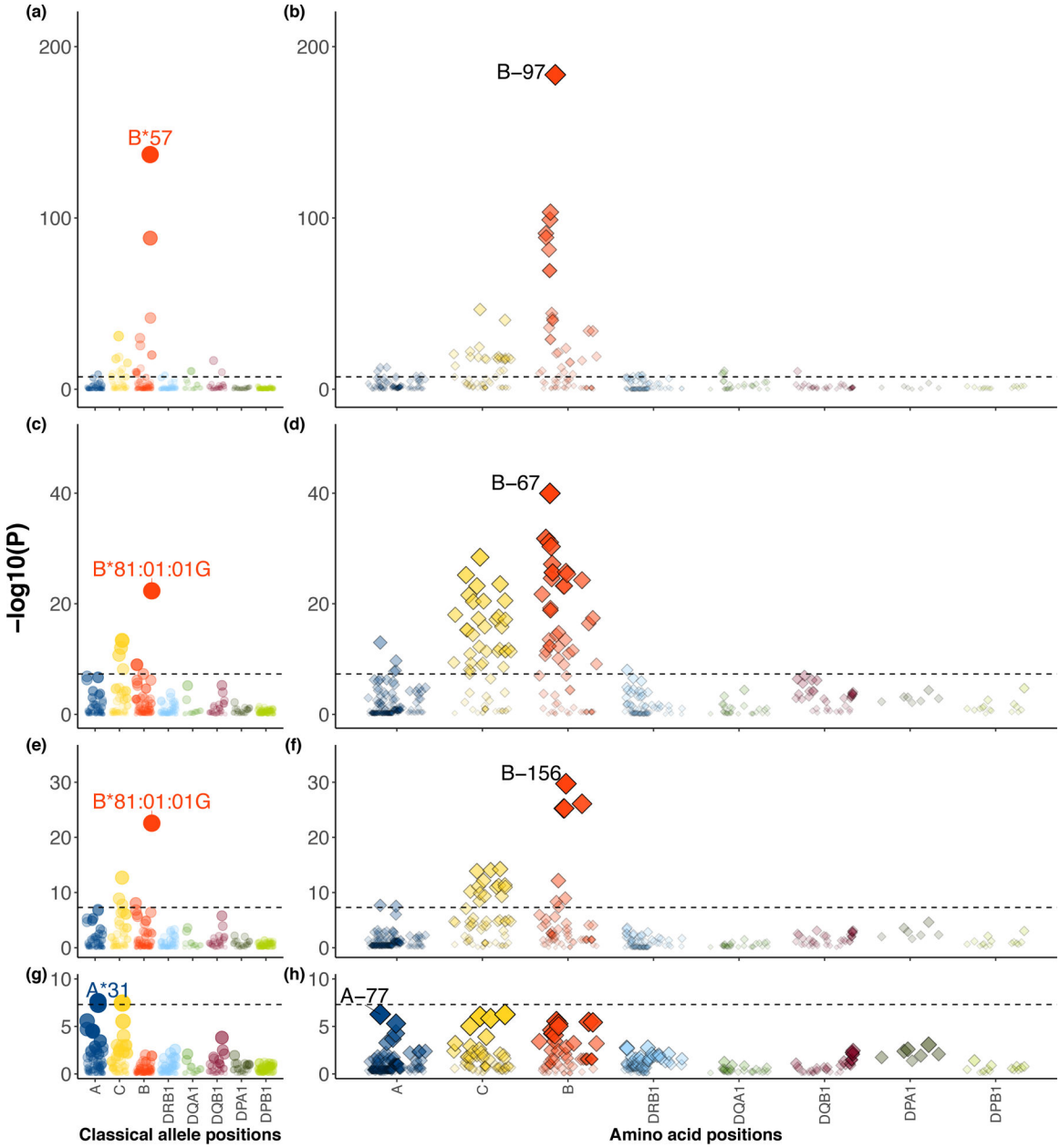

Figure 3 |. Stepwise conditional analysis of the allele and amino acid positions of classical HLA genes to HIV-1 viral load.

a-h, Each circle point represents the -$\log_{10}(P_{binary})$ from two-sided linear regression for all classical *HLA* alleles. Each diamond point represents -$\log_{10}(P_{omnibus})$ from one-sided F-test for the tested amino acid positions in HLA (blue, *HLA-A*; yellow, *HLA-C*; red, *HLA-B*; light blue, *HLA-DRB1*; green, *HLA-DQA1*; purple, *HLA-DQB1*, dark green, *HLA-DPA1*; light green, *HLA-DPB1*). Association at amino acid positions with more than two alleles was calculated using a multi-degree-of-freedom omnibus test. The dashed black line represents the significance threshold of $P = 5 \times 10^{-8}$ to correct for multiple comparisons (Bonferroni correction). Each panel shows the association plot in the process of stepwise conditional omnibus test. One-field classical allele *HLA-B*57* ($P = 9.84 \times 10^{-138}$) (**a**) and

amino acid position 97 in HLA-B ($P_{omnibus} = 1.86 \times 10^{-184}$) (**b**) showed the strongest association signal. Results conditioned on position 97 in HLA-B showed a secondary signal at classical allele *HLA-B*81:01:01:G* ($P = 4.53 \times 10^{-23}$) (**c**) and position 67 in HLA-B ($P_{omnibus} = 1.08 \times 10^{-40}$) (**d**). Results conditioned on position 97 and 67 in HLA-B showed the same classical allele *HLA-B*81:01:01G* ($P = 2.70 \times 10^{-23}$) (**e**) and third signal at position 156 in HLA-B ($P_{omnibus} = 1.92 \times 10^{-30}$) (**f**). Results conditioned on position 97, 67 and 156 in HLA-B showed a fourth signal at *HLA-A*31* ($P = 2.45 \times 10^{-8}$) (**g**) and position 77 in HLA-A ($P_{omnibus} = 5.35 \times 10^{-7}$) outside HLA-B (**h**).

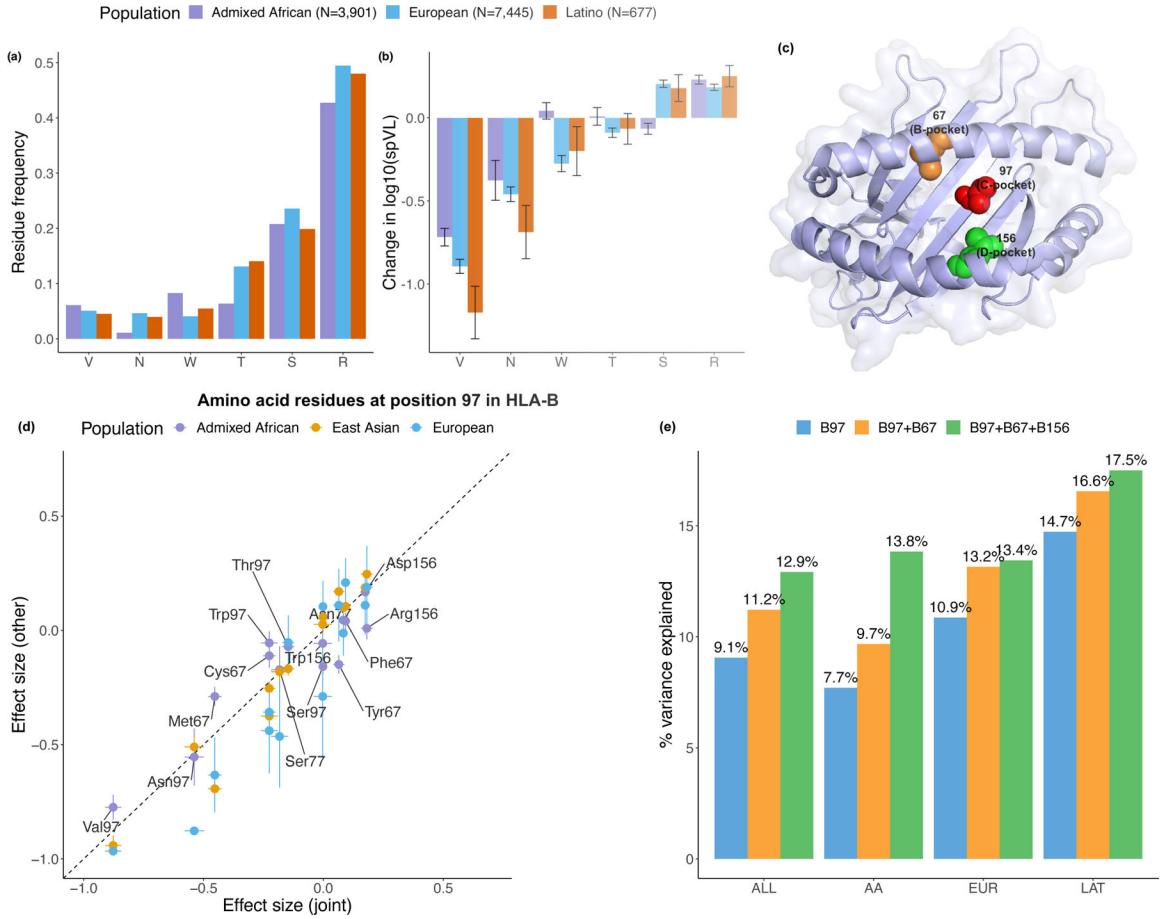

Figure 4 |. Location and effect of three independently associated amino acid positions in HLA-B.

a, Allele frequencies of six residues at position 97 in HLA-B among three populations. **b**, Effect on set point viral load (spVL) (i.e., change in $\log_{10}$ HIV-1 spVL per allele copy) of individual amino acid residues at position 97 in HLA-B. Results were calculated per allele using linear regression models, including gender and principal components within each ancestry as covariates. There are 3,901 Admixed African (purple), 7,455 European (blue) and 677 Latio (orange) independent samples included in the analysis. Data are presented as mean values (beta) ± standard errors. **c**, HLA-B (PDB ID code 2bvp) proteins. Omnibus and stepwise conditional analysis identified three independent amino acid positions (positions 97 (red), 67 (orange), and 156 (green) in HLA-B. **d**, Effect on spVL (i.e., change in $\log_{10}$ HIV-1 spVL per allele copy) of individual amino acid residues at each position reported in this and previous work[14,18]. Results were calculated per allele using linear regression models. The *x*-axis shows the effect size and its standard errors in the joint analysis, and the *y*-axis shows the effect sizes ± standard error in individual populations (purple, Admixed African, n = 3,901; blue, European, n = 7,455; orange, Latino, n = 677). **e**, Variance of spVL explained by the haplotypes formed by different amino acid positions.

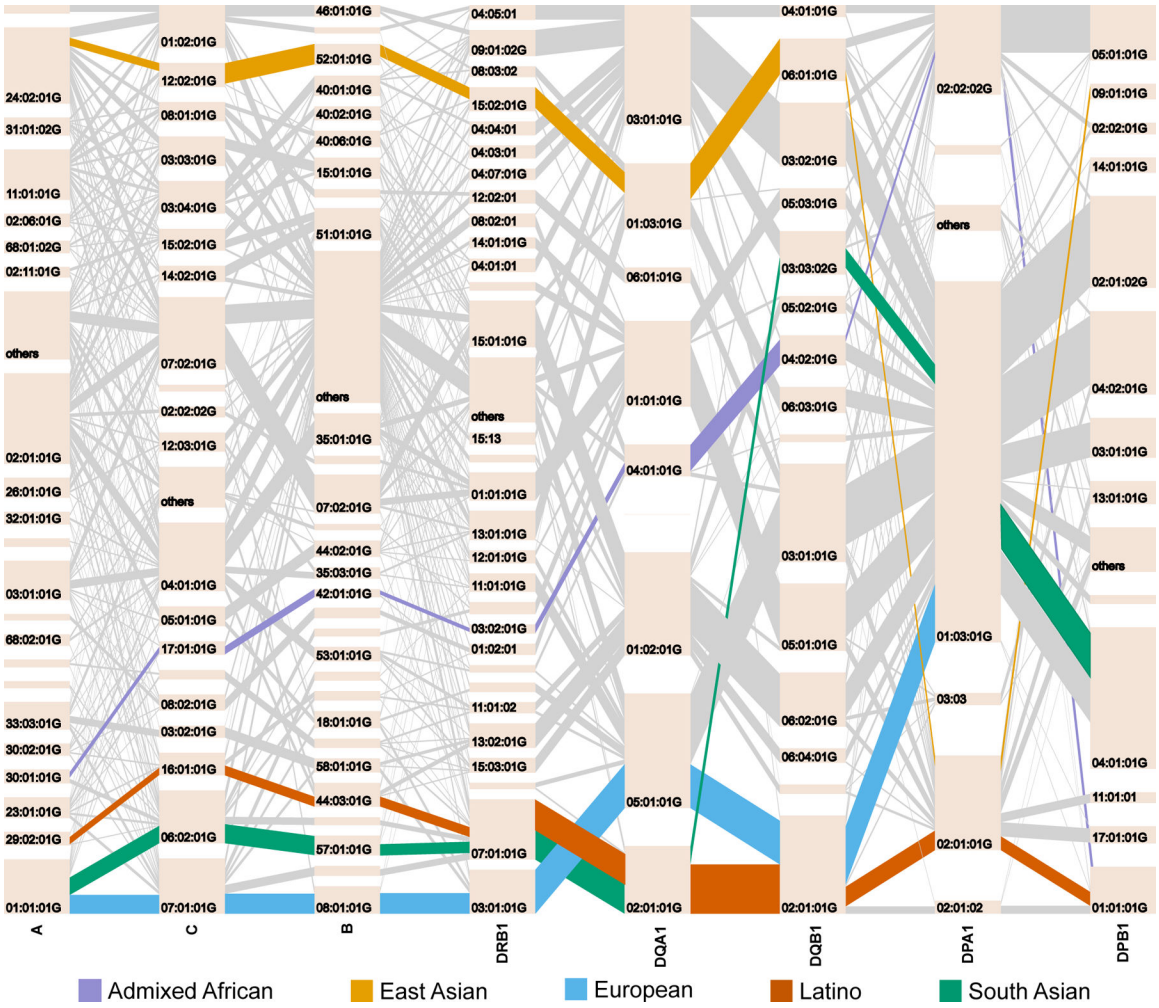

Figure 5 |. Pairwise LD and haplotype structure for eight classical HLA genes in five population groups.

Haplotype structures of the eight classical HLA genes in each population. The tile in a bar represents an *HLA* allele, and its height corresponds to the frequencies of the *HLA* allele. The gray lines connecting between two alleles represent *HLA* haplotypes. The width of these lines corresponds to the frequencies of the haplotypes. The most frequent long-range HLA haplotypes within each population is bolded and highlighted in a color described by the key at the bottom.

Table 1 |

Effect estimates for the haplotypes defined by the three independent amino acids in HLA-B associated with HIV-1 viral load.

Only haplotypes with >1% frequency in the overall population are listed (Supplementary Table 16). Classical alleles of HLA-B are grouped based on the amino acid residues presented at position 97, 67 and 156 in HLA-B. For each haplotype, the multivariate effect is given as an effect size, taking the most frequent haplotype (97R-67S-156L) as the reference (effect size = 0). Heterogeneity *P*-value (*P*(het), two-sided) of each haplotype is calculated using *F*-statistics with two degrees of freedom (Methods). Effect size and its standard error in each population are listed only for haplotypes that show evidence of heterogeneity ($P < 0.05/26$ Bonferroni-corrected for multiple tests, bolded). Unadjusted haplotype frequencies are given in each population.

HLA-B amino acid at position			Effect size (standard error)					Unadjusted allele frequency				Classical *HLA-B* allele
97	**67**	**156**	**AA**	**EUR**	**LAT**	**Joint**	***P*(het)**	**AA**	**EUR**	**LAT**	**Joint**	
V	M	L				−0.921 (0.036)	0.031	0.056	0.049	0.059	0.051	*B*57:01;B*57:03*
N	C	L				−0.554 (0.041)	0.257	0.012	0.046	0.037	0.035	*B*27:05*
T	S	L				−0.436 (0.041)	0.041	0.028	0.039	0.056	0.037	*B*13:02;B*52:01*
W	C	L				−0.397 (0.041)	0.581	0.03	0.039	0.054	0.037	*B*14:01;B*14:02*
S	S	L				−0.252 (0.066)	0.013	0.002	0.014	0.07	0.013	*B*40:02*
R	S	W				−0.177 (0.038)	0.618	0.009	0.062	0.028	0.044	*B*15:01;B*15:10;B*15:16*
T	F	L				−0.125 (0.036)	0.001	0.03	0.059	0.073	0.051	*B*51:01;B*78:01*
R	M	L				−0.125 (0.045)	0.375	0.061	0.014	0.028	0.029	*B*15:16;B*58:01*
R	C	L				−0.078 (0.039)	0.055	0.042	0.039	0.06	0.041	*B*15:10;B*15:16;B*39:10*
R	S	D	0.165 (0.056)	−0.07 (0.034)	−0.153 (0.173)	−0.019 (0.028)	**0.002**	0.075	0.108	0.084	0.097	*B*37:01;B*44:02;B*45:01*
R	S	L				Reference	0.536	0.191	0.176	0.197	0.18	*B*15:03;B*15:10;B*18:01;B*39:10;B*40:01;B*44:03;B*49:*
S	Y	D				0.015 (0.055)	0.884	0.059	NA	0.017	0.019	*B*42:01;B*42:02*
S	Y	R	−0.06 (0.055)	0.037 (0.033)	−0.002 (0.187)	0.022 (0.027)	**0.007**	0.08	0.124	0.07	0.108	*B*07:02;B*07:05*
S	F	D				0.041 (0.031)	0.218	0.034	0.095	0.042	0.074	*B*08:01*
R	F	L				0.045 (0.027)	0.73	0.182	0.095	0.113	0.122	*B*35:01;B*53:01*
W	M	L				0.098 (0.064)	0.268	0.046	NA	NA	0.014	*B*58:02*
T	Y	L				0.176 (0.058)	0.207	0.005	0.021	NA	0.016	